Colloidal Quantum Dot Solar Cells: Progressive Deposition Techniques and Future Prospects on Large-area Fabrication

*Qian Zhao**, *Rui Han*, *Ashley R. Marshall*, *Shuo Wang*, *Brian M. Wieliczka*, *Jian Ni*, *Jianjun Zhang*, *Jianyu Yuan*, *Joseph M. Luther*, *Abhijit Hazarika**, and *Guo-Ran Li**

Dr. Q. Zhao, S. Wang, Prof. G. R. Li

School of Materials Science and Engineering, Nankai University, Tianjin 300350, China

E-mail: qian.zhao@nankai.edu.cn; guoranli@nankai.edu.cn

Dr. A. Hazarika

Polymers and Functional Materials Division, CSIR-Indian Institute of Chemical Technology, Uppal Road, Tarnaka, Hyderabad 500007, India

E-mail: abhijit@iict.res.in

R. Han, Dr. J. Ni, Pro. J. Zhang

College of Electronic Information and Optical Engineering, Nankai University, Tianjin 300350, China

Dr. A. R. Marshall

Condensed Matter Physics, Department of Physics, University of Oxford, Parks Road, Oxford OX1 3PU, UK

Dr. B. M. Wieliczka, Dr. J. M. Luther

National Renewable Energy Laboratory, Golden, CO 80401, USA

This article has been accepted for publication and undergone full peer review but has not been through the copyediting, typesetting, pagination and proofreading process, which may lead to differences between this version and the Version of Record. Please cite this article as doi: 10.1002/adma.202107888.

Prof. J. Yuan,
Institute of Functional Nano & Soft Materials, Jiangsu Key Laboratory for Carbon-Based Functional Materials & Devices, Soochow University, Suzhou, Jiangsu 215123, China

Keywords: colloidal quantum dot, deposition technique, scale-up, perovskite, solar cell

Abstract

Colloidally grown nanosized semiconductors yield extremely high-quality optoelectronic materials. Many examples have pointed to near perfect photoluminescence quantum yields, meaning non-radiative optical processes (losses) can be completely suppressed allowing for technology-leading materials as high purity color centers in display technology and emitters in LEDs. Furthermore, because of high chemical yield, and improved understanding of the surfaces, these materials, particularly colloidal quantum dots (QDs) can also be ideal candidates for other optoelectronic applications. Given the strong drive toward carbon neutrality and limiting climate change, electricity from solar photovoltaics will play a large role in the power generation sector. QDs have been developed and shown dramatic improvements over the past 15 years as photoactive materials in photovoltaics and have unique potential with various innovative deposition properties which could lead to exceptionally low-cost and high-performance devices. Once the key issues related to charge transport in optically thick arrays are addressed, QD-based photovoltaic technology could become a better candidate for practical application. In this article, we show how the possibilities of different deposition techniques could bring QD-based solar cells to the industrial level and discuss the challenges for perovskite QD solar cells in particular, to achieve large-area fabrication for further advancing technology to solve pivotal energy and environmental issues.

1. Introduction

Maturing any proof-of-concept technology from laboratory to commercial scale manufacturing is not an easy task. Processes developed for lab-scale demonstration can be specifically optimized at small size and are often not applicable as the product is scaled. In photovoltaic (PV) research and industry, large-area fabrication without compromising the power conversion efficiency (PCE) always comes with new and unexpected challenges even for well-studied and well-optimized laboratory-scale PV technologies. For instance, non-concentrated monocrystalline silicon solar cells have reached a record 26.1% PCE,[1] but the efficiencies of most recent commercial panels are typically only up to about 22% (e.g., SunPower's Maxeon 3 panels: 22.8%, LG's Neon R: 22%, Panasonic's EverVolt: 21.7%).[2] Apart from the technical challenges, cost is the main driving factor for industry when it comes to production of modules or panels by scaling up laboratory-scale research cells. Low-cost PV technologies with performance comparable to existing industrial PV technologies may help in achieving the desired cost target, and perovskite solar cell (PSC) technology is the most suitable candidate in the current scenario.[3] The last decade saw a monumental rise in PSC technology. The perovskite absorber naturally possesses most of the desired properties for highly efficient solar cells, such as long carrier diffusion length, high carrier mobility, high light absorption coefficient and excellent defect-tolerance.[4] Both in terms of laboratory-scale research cells and large-area panels, PSCs have seen steep rise in PCE, reaching 25.8% for research cells,[1] and 17.9% for large-area modules with size of 802 cm^2.[2] Further, PSC processing is relatively simple and inexpensive, raising the hopes that PSCs will lead to wide-spread deployment of solar power. Based on the recent technoeconomic analysis by Heben et al., the direct manufacturing cost of a 16% efficient perovskite PV module is \$31.7 per m^2 with a minimum sustainable price of \$0.41 per Wp (watt per peak), which makes PSC a low-cost leader in PVs.[5] And with GCL New Energy launching a 100 MW-capacity production line for 18%-efficiency PSC modules with a 70% lower production cost than that of the crystalline-Si,[6] and Saule Technologies recently in May 2021 launching a commercial production line for PSCs in Wroclaw, Poland,[7] PSC PV technology has taken a big leap towards commercialization.

Colloidal quantum dots (CQDs), particularly the metal chalcogenides (e.g., CdSe) have already stormed into the display market with substantial commercial success due to their exceptional brightness, color purity and color gamut. Examples are quantum dot-based LED TVs manufactured and marketed by leading companies like Samsung and Philips. In the area of PV technologies, quantum dot solar cells (QDSCs) have attracted attention as low-cost solution processable alternative much before the invent and rise of bulk lead halide perovskites.[8] With continued development, QDSCs have reached 18.1% efficiency in 2021.[1] Before 2015, the CQD PV technology was dominated by the lead chalcogenide family (PbS and

PbSe). Immediately after the hot-injection synthesis of colloidal lead halide perovskite QDs (PQDs) was reported,[9] PQDs became the dominant absorber material in QDSCs. PQDs combine many of the characteristics of traditional metal chalcogenide CQDs, such as quantum confinement and passivation of surfaces by ligands, with the exceptional PV properties of bulk lead halide perovskite semiconductors. Compared to bulk/thin film-based PSCs that are mostly processed from hazardous DMSO and DMF,[10] QDSCs offer a unique advantage: they are compatible with and processed using greener solvents (e.g., hexane, octane, toluene, etc.). Low-cost solution-state processing, (in particular, the availability of various simple deposition techniques such as spray coating and doctor blading that are feasible to use in roll-to-roll processing) is one of the most attractive attributes of PSCs and QDSCs as an alternative to silicon PV. In addition, the compatibility of CQDs with greener solvents is somewhat advantageous over bulk perovskites when large-scale industrial fabrication is considered. Even with such desirable advantages, it may be exaggerated to think or claim at this moment that CQD-based PV technology will immediately replace the well-established Si PV technology or the emerging PSC technology until they match in terms of PCE of large area modules or panels. But this is not unreasonable to envision such a scenario given CQDs' commercial success in display and lighting technologies. In the field of solar energy utilization, luminescence solar concentrators (LSCs) using CQDs offer promising alternative applications.[11] Such LSCs can be integrated with Si-solar cells in tandem, even for large-area applications like glass windows.[12] Prototype solar windows developed by QD manufacturing start-up UbiQD Inc. are being durability tested at NREL for future wide-spread applications in smart-building industries.[13] More recently, the same start-up company has taken the CQDs into new applications by designing QD-enabled greenhouse films, which they term as "UbiGro".[14] Funded by NASA for potential space applications, UbiQD in collaboration with NanoSys is already marketing these films, as well as luminescent lanterns for optimizing sunlight in greenhouses.[15] Such industrial scale progress of CQD based technologies support novel commercialization of QD PV technologies. Moreover, the ability to achieve any band gap in the electromagnetic spectrum by size and/or composition tuning, along with the ability to form heterojunction architectures,[16] the CQDs are ideal either for top cell or bottom cell for tandem solar cells of different configurations like QD–QD tandem, QD–PSC tandem, Organic dye–QD tandem.[17] CQDs can offer suitable solutions to a few bottlenecks currently suffered by tandem solar cells involving thin-film halide perovskites. The Si–perovskite and perovskite–perovskite tandem solar cells utilize wide-bandgap perovskite absorbers of appropriate bandgaps (~1.66–1.77 eV) as the top-cell, and these wide-bandgap perovskite compositions contain mixed halides (bromide and iodide) as the X-site anions. But mixed halide perovskites are known to undergo photoinduced halide phase segregation that typically leads to voltage loss. Colloidal PQDs can achieve such bandgaps suitable for tandem top-cell without necessarily having mixed halides,[18] thus making them suitable candidates for such applications. Further, in the perovskite–perovskite tandem solar cell architecture, the bottom cell necessarily contains Sn-based perovskite compositions as narrow band-gap absorber. The Sn-based perovskites typically have lower absorption cross-sections as compared to pure Pb-based perovskites, thus demanding a thickness higher than 1 μm for attaining a higher current density or quantum efficiency.[19] This is not trivial for thin film perovskites, as crystallizing large enough grains from molecular precursors requires extensive optimization. Colloidal PQDs here may become advantageous, as any thickness of CQD solid films can be achieved by layer-by-layer (LBL) deposition. Although there is no report so far for Si–QD tandem architecture similar to Oxford PV's PSC–Si tandem cells, there is no fundamental reason why such possibility cannot exist. So overall, with all these positive developments, it is realistic to project CQD-based PV technology for commercial applications.

If we compare the fabrication process of QDSCs and thin film PSCs, all the layers are deposited in a similar manner except the main absorber layer. In thin film PSCs, the perovskite absorber layer is typically deposited from polar solvents like DMF and/or DMSO followed by an antisolvent (e.g., toluene) treatment and subsequent annealing that converts the molecular precursors into perovskite crystals. The quality of the absorber layer and the overall efficiency of the PSCs strongly depend on the crystallization dynamics, and therefore the deposition parameters are very crucial. On the other hand, in QDSCs, the quantum dot absorber layer is typically deposited from a non-polar solvent like octane or hexane in a LBL approach accompanied by intermediate solid-state ligand exchange, or using a one-step deposition method where ligand exchange is done in solution prior to deposition.[20] Since the absorber material is already in crystalline form in the CQD ink, the quality of the absorber layer and PV performances of the QDSCs depend on the surface chemistry of QDs and effective inter-dot coupling. Once the PCE of halide perovskite-based QDSCs matches that of thin film-based PSCs (~25%), the above-mentioned advantages of QDSCs could make a significant difference in the field of solution processable PV technology. Moving towards that goal, the open circuit voltage (V_{oc}) of the QDSCs is already comparable, often demonstrating less loss compared to the thin film-based PSCs,[18,21] and the main parameter that needs significant improvement is the current density (J_{sc}). Different deposition techniques for QDSCs, particularly those relevant for large-area fabrication, and ligand exchange steps, are expected to affect the current density.

One of the most crucial components of QDSC fabrication is CQD processing by surface chemistry manipulation, that is replacement of insulating long-chain organic ligands with atomic/inorganic/small organic molecular ligands. This step strictly dictates the QD electronic coupling and surface trap density, film uniformity, roughness and compactness.[22] This ligand replacement is generally done either in solution phase or by "solid state" ligand exchange. In solution phase ligand exchange, the long-chain organic ligand capped CQDs are treated with a solution containing the small ligands. The final ink generated by this approach is used for a one-step deposition process for QDSCs. In case of solid-state ligand exchange, the long-chain organic ligand capped CQDs are first deposited on the substrate, and then treated with the solution containing the small ligands to replace the native ligands on the CQD surface. Repetition of this process several times results in the desired thickness of the final absorber layer in the QDSCs. For the one-step deposition, the whole procedure is relatively easy since the ligand exchange is not involved in the deposition process and the resulting film thickness is mainly determined by the concentration of the QDs in the colloidal solution. On the other hand, the LBL method enables the modifications of QD surfaces *via* treatment between each QD layer, creating the opportunity to boost the quality of QD films during the deposition process.[23] The complete CQD LBL deposition technique can be described in three general steps as depicted schematically in Figure 1: (1) The as-synthesized CQDs with long-chain organic ligands are purified multiple times and then dispersed in a suitable non-polar solvent in the desired concentration, which is then deposited on a pre-cleaned substrate of choice (Figure 1a), forming a wet QD film (Figure 1b). (2) The solvent in the QD film dries and a solid QD film is formed where the individual QDs are separated by the organic capping ligands (Figure 1c). Such QD solid films are not ideal for charge transport as there is minimal carrier wave function overlap due to the wide-spacing of the QDs. (3) To overcome the carrier transport issue and produce a strong electronically coupled QD film, the long-chain ligands are replaced with short ligands (Figure 1d) and rinsed off from the QD films using a nonsolvent that does not disperse or dissolve the QDs. A neat and compact solid QD film with short ligands covering the surface is achieved once the nonsolvent evaporates (Figure 1e). It should be noted that the chemistry involved in deposition mainly depends on the compositions of QDs and the applied ligands. Once the ligand exchange is complete the QDs in the film are no longer soluble in the deposition solvent and the entire procedure can be repeated as desired to yield a target thickness of QD films. It is also worth mentioning here that such thickness control of the absorber layer that can easily be achieved in QDSCs using LBL method, particularly forming a thick (over one micron) layer with smooth morphology is challenging in case of thin-film based PSCs.

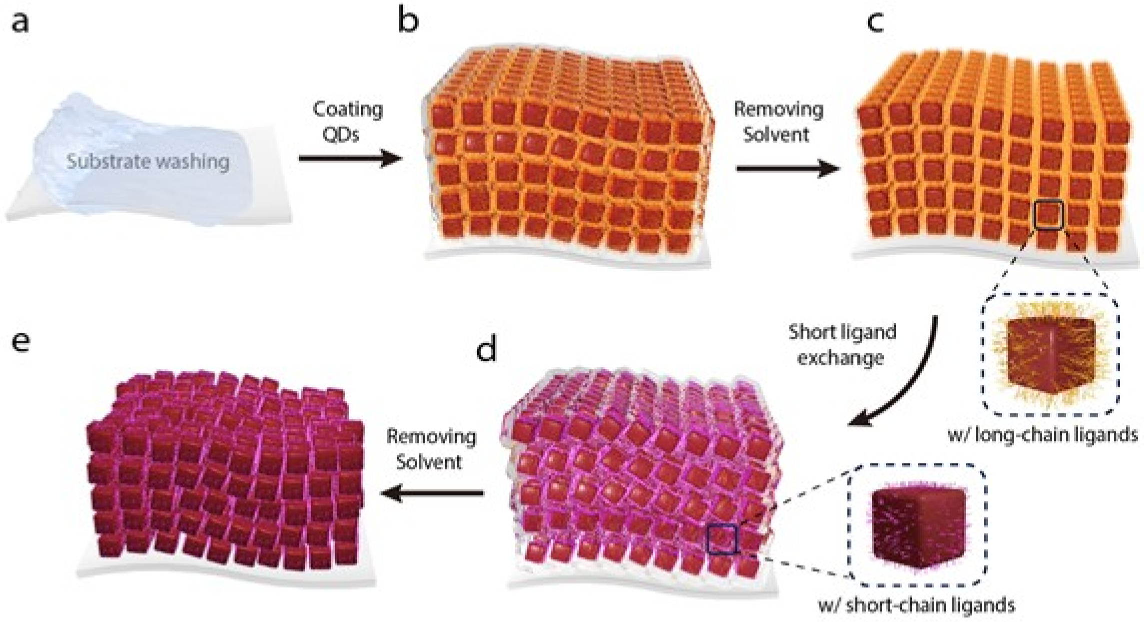

Figure 1. a-e) Schematic representation of QD depositing procedure including: substrate cleaning (a), deposition of QD layer to form a wet layer (b), solvent drying to form a dry QD layer where each QD is separated by long-chain organic ligands (c), treatment with a solution containing short ligands (d), solvent drying to form a compact QD film where each QD is electronically coupled through short ligands (e).

This LBL deposition method involving solid-state ligand exchange, however, disrupts the physical and chemical integrity of the CQD film in a number of ways: (i) Increased exposure time to atmosphere leads to oxidation of the QDs, resulting in non-radiative charge-carrier recombination on QD surface and can cause decomposition or phase change of QDs.[24] (ii) Solid-state ligand exchange procedure may degrade or reduce surface, which can also generate an increased surface trap density.[25] (iii) The replacement of long-chain ligands using much shorter ligands breaks the long-range ordered assembly in the initial QD films resulting in variation of dot-to-dot spacing. Since carrier transport takes place along the most efficient and shortest path, nonuniform interdot spacing causes a nonuniform transport that could affect the photogenerated carrier mobility and lifetime in PVs.[26] (iv) The film volume decreases after long organic molecules on the QDs are exchanged with short ligands, which dramatically increases the roughness and discontinuity of the prepared film resulting in a reduced film density, low absorption per unit length and potential electrical shorts.[26,27] Moreover, the LBL process is not ideal for achieving optimal absorber layer thickness since this process wastes large volumes of solvents and energy, increasing the fabrication costs.[28] Multiple deposition steps are expected to generate a huge amount of toxic hazardous waste because the typical QD inks currently being used in QDSCs contain heavy metals, which hinders the industrialization of QDSCs. Numerous efforts over recent years have been made to overcome these challenges and fulfill the goal of depositing a QD film with high compactness, passivated recombination centers and enhanced carrier mobility.[23c,29] In this review, we highlight the history and background of different CQD deposition techniques which are either already being used or have potential in QDSCs fabrication. We will also discuss some recent advances in these deposition techniques and each of their pros and cons with a focus on potential for large-area fabrication. We will finally address the unique advantages and challenges when it comes to the emerging perovskite QDSCs in particular.

2. CQD Deposition Techniques

CQDs can be utilized to fabricate a variety of solar cells with different architectures, such as Schottky junction,[8d,30] heterojunction,[23b,24a,31] quantum junction or nano-heterojunction,[16,32] quantum funnels[33] and tandem solar cells.[17a,17d,34] Although the overall charge transport mechanism is distinctly different when employing different device architectures, the requirement of a highly compact and uniform QD absorber layer with excellent optoelectronic properties remains universal in all types of devices, and this is mainly influenced by the CQD deposition methods. As discussed in the introduction, one of the major criteria of a high quality CQD film is proper control of the surface chemistry, since this facilitates charge transport and surface defect passivation. This can be achieved by replacing the native insulating ligands on the CQD surface without compromising the defect passivation. The QD surface manipulation strategies (solution phase or solid state ligand exchange) are common irrespective of the deposition techniques, although a variety of ligand types and/or interfacial layers have been reported. We will highlight such optimization processes during the solar cell fabrication process while discussing different deposition techniques. Since spin-coating is the most-widely used method for fabricating and optimizing any lab-scale solar cells, we will start our discussion with QDSCs fabricated using spin coating.

2.1 Spin Coating

The spin coating technique is one of the most common, established, and easily accessible wet coating methods with crucial advantages over other coating methods. The high spin speed and airflow employed during spin casting leads to fast drying of the solvent resulting in smooth and continuous QD films. Spin coating is a small-area deposition method with good control of operating parameters for fundamental research and lab-scale device fabrications. Most of the reported QDSCs are typically fabricated by spin-coating techniques and the latest published research cell record efficiency of 16.6% has been obtained using spin coating.[35] In addition to the CQD absorber layer, the electron transport and hole transport layers (ETL and HTL) of the QDSC are also deposited using spin coating. Spin coating consists of several stages: fluid dispense, spin up, stable fluid outflow, spin off, and evaporation (Figure 2a-c). For QD deposition, the ligand-capped CQD solution must be prepared in the right concentration in a suitable solvent. Then, as displayed in Figure 2a-c, the CQD solution is dispensed onto the substrate mounted on a rotating vacuum stage, and subsequently spread and sheared through the centrifugal force generated by the high-speed rotation. This process forms a gelatinous network on the substrate surface and the subsequent drying of solvent solidifies the CQD gel, resulting in a solid film. The electrical properties and morphologies of the resultant QD film are highly sensitive to spin speed and ambient conditions like temperature and humidity during the spin coating process. The thickness of a QD layer, h, deposited by spin coating can be calculated by the following equation:[36]

$$h = \left(1 - \frac{\rho_A}{\rho_{A0}}\right)\left(\frac{3nm}{2\rho_{A0}\omega^2}\right)^{1/3} \tag{1}$$

Where ρ_A is the density of the volatile liquid, ρ_{A0} is the initial density of the volatile liquid at the onset of spin off, n is the viscosity of the QD solution, m is the rate of evaporation, and ω is the angular speed of rotation.

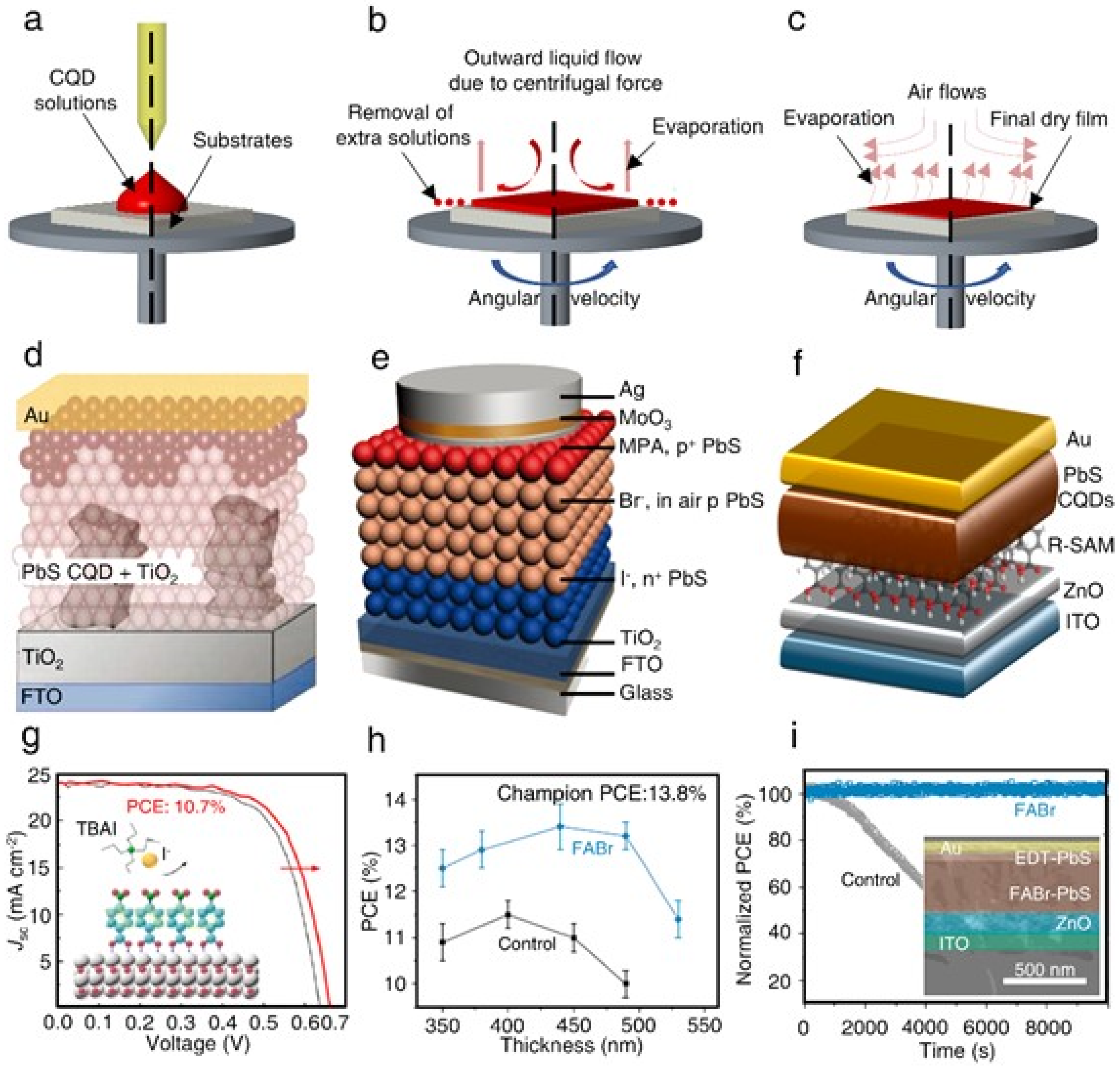

Figure 2. a-c) Schematic illustration of spin coating process showing the different steps involved. d) Schematic drawings of the cross-section of depleted bulk heterojunction PbS QD solar cells. e) Schematics of inverted quantum junction PbS QD solar cells with a color gradient indicating the charge depleted portion of the device using mercaptopropionic acid, bromide and iodide for the solid-state ligand exchange. f) Schematic of a prototypical PbS QD device structure including a SAM between the ZnO and the PbS CQD film. g) *J–V* curves of PbS QD devices with 4-aminobenzoic acid R-SAMs. Inset is the schematic drawing of the ligand

exchange process using tetrabutylammonium iodide. h) PQD thickness-dependent PCE for FABr-treated and untreated PbS QD films. i) Operating stability of FABr-treated and untreated PbS QD devices under continuous AM1.5G illumination. Inset is the cross-section SEM image of the used device structure. d) Reproduced with permission.[23b] Copyright 2011, Wiley-VCH. e) Reproduced with permission.[37] Copyright 2014, Nature Publishing Group. f-g) Reproduced with permission.[38] Copyright 2015, American Chemical Society. h-i) Reproduced with permission.[39] Copyright 2020, Elsevier.

Over the past 15 years, CQD solar cells fabricated by spin coating have experienced significant PCE improvement through device architecture engineering,[16,17a,30,31b,33c] surface chemistry control[23c,40] and modifications of structured electrodes[31a,41] for efficient photocarrier separation and collection. McDonald et al. reported the very first infrared QDSC in which spin coating was employed to deposit a polymer–PbS CQD composite film.[42] Originally, CQDs attracted a lot of attention as sensitizers in quantum dot sensitized solar cells, which resemble the molecular dye sensitized solar cells.[43] Devices with solid CQD films as the absorber layer soon came into the limelight and device structures that resembled the polycrystalline semiconductor analogues became the most common QDSCs.[44] Based on LBL spin coating, Sargent et al. established the first solution-processed depleted bulk heterojunction solar cells using PbS CQDs with an optimized mesoporous TiO_2 layer to enhance absorption without compromising electron extraction (Figure 2d), and reported a CQD PV efficiency of 5.5% under simulated AM1.5 illumination.[23b] Moreover, Tang et al. demonstrated an atomic ligand exchange strategy that employs monovalent halide anions to enhance charge transport and passivate surface defects in QD films. This strategy, spin coating PbS QDs and subsequently treating the QD film with a solution of cetyltrimethylammonium bromide (CTAB), showed an improvement in PCE to 6%.[40a] In 2012, Sargent's group further demonstrated a solution phase ligand exchange to fabricate QDSCs to reduce mid bandgap trap states resulting in an enhanced PCE (certified) reaching 7%.[40c]

One major advantage of the ability to deposit the CQDs in LBL fashion is that band alignment engineering within the QD absorber film can be carried out by depositing the CQDs with the same chemical composition but with different types of carrier doping (n- or p-type) as the different QD layers inside. Such variations in doping can be achieved by using different types of surface ligands during the ligand exchange approach. For instance, PbS CQDs treated with mercaptopropionic acid (MPA) results in p-doped films, bromide (in a N_2 atmosphere) leads to n-doping, bromide (in air) to p-doping, iodide to n-doping and hydroxide to p-doping. These different treatments of PbS CQDs can be successively stacked together in one QD solid film (Figure 2e) to give a thicker depletion region that extends the carrier transport length.[37] Similarly, solar cells with two PbS QD treatments – tetrabutylammonium iodide (TBAI) and 1,2-ethanedithiol (EDT) – form a heterostructured QD absorber layer that achieved a certified efficiency record of 8.55% for QDSCs in 2014.[45] Molecular iodine, methylammonium iodide or a perovskite thin shell can also be used to treat PbS QD. Many of these treatment strategies focus on the passivation of trap states at the QD surface and are beneficial to enhancing the V_{oc} of QDSCs. The enhancement of V_{oc} has been seen as the most quantitatively significant opportunity for improved PbS QDSC performance.[46]

Apart from CQD surface engineering, a number of interface passivation strategies have been developed to tackle the interfacial charge recombination in spin coated QDSCs. Inserting a buffer layer at the CQD/ETL interface can effectively reduce interfacial charge recombination, improve electron extraction, and further enhance the external quantum efficiency (EQE).[47] For instance, heterojunction QDSCs with PCBM as buffer layer between the TiO_2 and PbS CQD layers obtained a PCE of 8.9%.[48] The insertion of a self-assembled monolayer (R-SAM) between PbS QD and ZnO layers (see Figure 2f-g) has shown to help optimized the band alignment at this interface, resulting in efficient charge extraction and a remarkable PCE of 10.7%.[38] Chloride passivated ZnO exhibiting decreased surface trap densities also offered a favorable electronic band alignment in PbS QDSCs.[41c] When In^{3+}-doped ZnO is used as the ETL with an n-type CQD : p-type CQD bilayer, a double-side junction device is formed that minimizes charge recombination and maximizes fill factor (FF) in PbS QDSCs; resulting in a PCE of 10.8%.[49]

Recently, Choi et al. demonstrated a homogeneous PbS CQD bulk homojunction film by blending n-type CQD with p-type CQD prior to spin coating. This enabled a 1.5-fold increase in carrier diffusion length as compared to the previous best CQD films fabricated via a cascade surface modification scheme and boosted the PCE of the PbS CQD solar cells to 13.3%.[32c] Passivating the surface of lead chalcogenide CQDs with halide perovskite materials has been shown to increase the inter-QD coupling, and thus substantially increase the carrier diffusion length as compared to pristine lead chalcogenide QD solid films. Such perovskite passivation can be achieved by treating the CQD layer with halide salts, as demonstrated by Sun et al., where they grew a monolayer of halide perovskite on PbS QD surface by FABr treatment achieving a PCE up to 13.8% that is the current record for Pb chalcogenide QDSCs with significantly enhanced operating stability (Figure 2h-i).[39]

From the above example of QDSCs, one can understand that spin coating is an ideal fabrication method that gives ample opportunity to play around with different parameters for optimized performance, such as surface treatment, film thickness, and doping. This can be considered a testing platform for translating these technical advances to large-area modules and practical applications. Some disadvantages of solar cell fabrication by spin coating are likely to be common with large area module fabrication. For example, emerging PQD solar cells in recent times are primarily fabricated using spin coating and, unavoidably thus far, use costly chemicals like methyl acetate. When scaling up to large area fabrication, the consumption of methyl acetate is expected to enormously increase the overall cost. Therefore, research must be done to find an alternative, low-cost chemical to enable scale-up of this process. Likewise, ligand exchange during the LBL spin-coating process breaks the long-range ordering of QDs, yet the ligand exchange is an unavoidable step regardless of deposition technique. Some efforts made on the CQD self-assembly process have shown that this problem can be rectified by modifying the dispersion properties of QD solutions such as particle weight fraction, solvent volatility and solvent viscosity etc.[50]

However, some challenges associated with spin coating can be avoided in other deposition techniques. For instance, spin coating process wastes a significant fraction of the total CQD solution and is likely not conducive to scaled-up device fabrication for the commercialization of CQDs solar cells.[22] This problem can be solved in other deposition techniques involving droplet-based methods like spray coating and inkjet printing, as well as liquid film-based methods such as blade-coating and slot-die coating. Commendable efforts have already been made towards scalable, large-area QDSCs involving such deposition technologies and we will focus on these deposition techniques next.[51]

2.2 Drop Coating & Dip Coating

The other two most commonly used small-scale, batch-processing methods are drop coating and dip coating. Drop coating is the simplest and easiest method among all of the developed CQD deposition methods. In this process, as shown in Figure 3a, a drop of CQD solution is directly deposited on the substrate, and the solvent is left to evaporate completely, forming a QD film. The utilization rate of the material for drop coating can reach nearly 100%.[52] In 2013, Fischer et al. fabricated a PbS QD solar cell through single-step drop coating, resulting in a PCE of 2.1% (Figure 3b).[20a] However, due to a lack of adequate control over film formation, the quality of the drop coated film is not sufficient for applications in high-efficiency optoelectronic devices.[53] As presented in Figure 3c, large cracks and nonuniformity are observed in the drop coated PbS QD film, while the spin coated counterparts are nearly uniform and crack-free. To make the drop coating technique more effective and versatile, further optimizations of the solvent evaporation and the diffusion of the CQDs on substrate surface are required, which should produce better film morphology and result in better performance of the final QDSC.

The dip coating process, in general, can be schematically described in five steps as shown in Figure 3d: (1) Immersion: the bare substrate is immersed into the CQD solution; (2) Extraction: the immersed substrate is withdrawn from CQD solution forming a boundary layer; (3) Deposition & (4) Drainage: the deposition and drainage take place simultaneously; (5) Evaporation: the solvent evaporates from the wet film leaving behind a dry QD film. When the system is kept in the Newtonian regime, which depends on the withdrawal speed, the thickness of the coated layer can be expressed using the Landau-Levich equation:[54]

$$h = 0.94\frac{(nv)^{2/3}}{y_{LV}^{1/6}(\rho g)^{1/2}} \qquad (2)$$

where h, n, v, y_{LV}, ρ, and g represent the coating thickness, withdrawal speed, viscosity, liquid-vapored surface tension, density and gravity; respectively. The dip coating method is not only simple and low-cost, but also very tolerant to the shape of the substrate including plane or curved surfaces and complex substrate shapes.[56] Furthermore, compared to spin coating and drop casting, LBL dip coating assembly can suppress the formation of cracks and achieve excellent control over the QD film thickness in a large area.[57] The dip coating method has been developed and used to deposit QD absorber layers in solar cells for decades.[58] The first QD solar cell with a certified 1-sun conversion efficiency of 2.94% reported by Luther et al. in 2010 was fabricated by dip coating PbS QDs on ZnO nanoparticles.[44b] In 2008, the first Schottky solar cells based on CQD films were also established by LBL dip coating, which achieved an AM1.5G PCE of 2.1%.[30] Crisp et al. reported dip coating PbS and PbSe QDSCs using a metal halide ligand exchange, with QD film thicknesses approaching one micron and a PCE of 7.25% (Figure 3e-g).[40e] Similarly, Zhang et al. introduced cesium lead halide QDs to passivate PbSe QDs via ion exchange[59] or as a back layer in a bilayer structure[60] during dip coating process, and further improved the PCE of PbSe QDSC to 8.2%.

Nonetheless, the main obstacle to scaling-up dip coating for QDSCs is that it is difficult to precisely control film thickness when using highly diluted or highly viscous solutions for ultra-thin (<20 nm) or ultra-thick (>1000 nm) QD films.[61] Another important obstacle is material shrinkage during drying and consolidation steps, often leading to cracks in QD films; especially for the wet QD films when the adhesion forces of the QD film on the substrate is not strong enough to overcome the lateral tensile stresses.[61,62] In addition, the wet film formed during dip coating is susceptible to changes in environmental factors like temperature and relative humidity,[63] which also need to be addressed when dip coating is employed. Such small-scale batch-processing methods described above are more appropriate for initial research purposes, but for large-area coating, the feasibility of scaled-up CQD manufacturing must be considered and improved to be compatible with roll-to-roll processing.

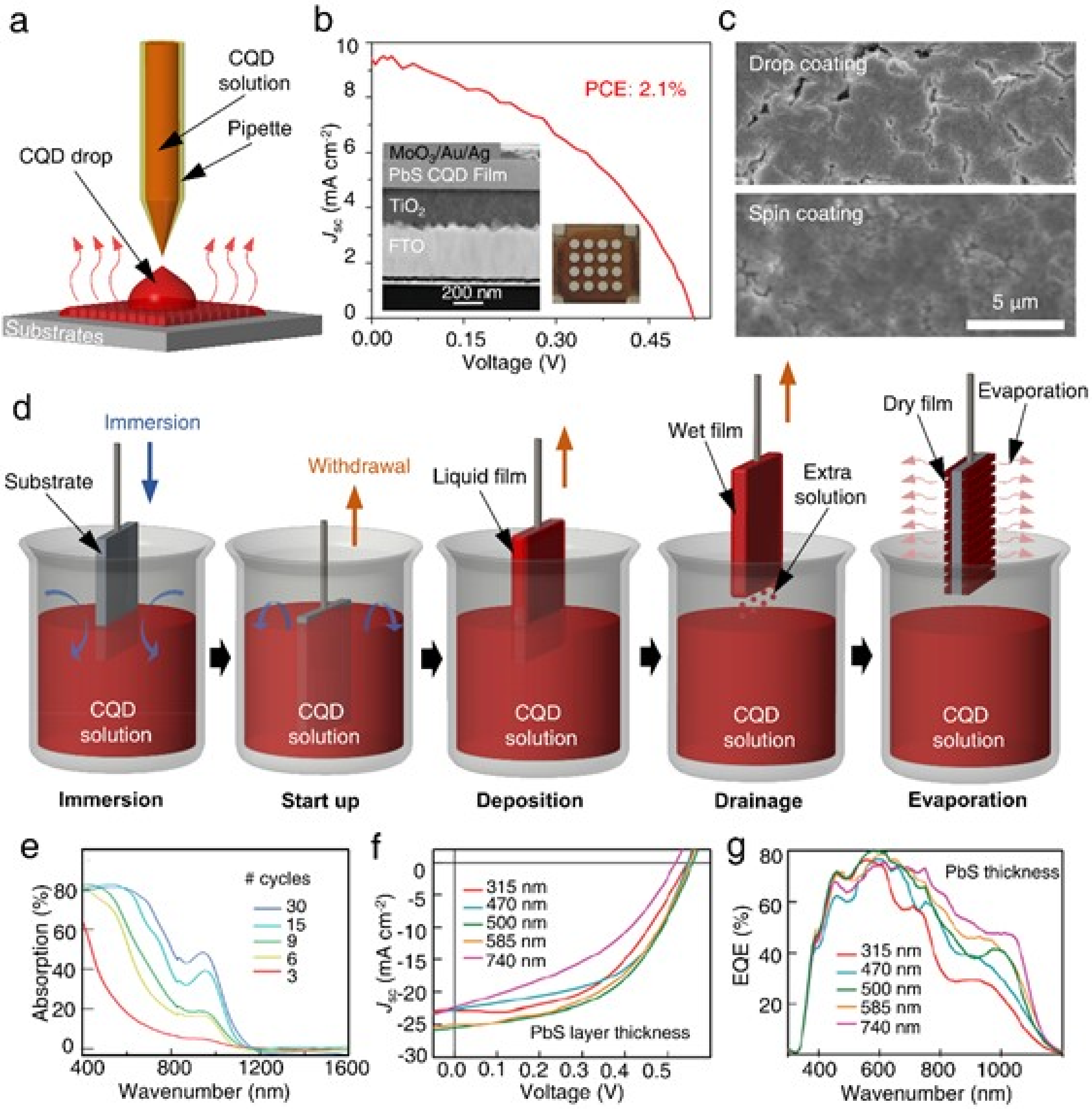

Figure 3. a) Schematic of drop coating process. b) *J–V* curves of the PbS QDSC fabricated by single-layer drop coating, leading to a PCE of 2.1%. Insets are a cross-sectional TEM image of the device structure and a photograph of a drop coated QDSC. c) Comparative SEM images of PbS QD films deposited by spin coating and drop coating. d) Schematic illustration of dip coating process. e) Absorption spectra of dip coated PbS QD films on glass as a function of the number of dip cycles with a PbI_2 ligand exchange. f-g) *J–V* curves (f) and EQE spectra (g) as a function of QD film thickness for PbI_2 dip-treated devices. b) Reproduced with permission.[20a] Copyright 2013, Wiley-VCH. c) Reproduced under the terms of Creative Commons CC BY license.[55] e-g) Reproduced under the terms of Creative Commons CC BY license.[40e]

2.3 Spray Coating

The development of spray coating is motivated by the need for rapid deposition in roll-to-roll device production and high material transfer efficiency. Spray coating is a deposition method without centrifugal force (as with spin coating), enabling large-area coatings on a wide variety of substrates such as planar, curved, and mesh surfaces.

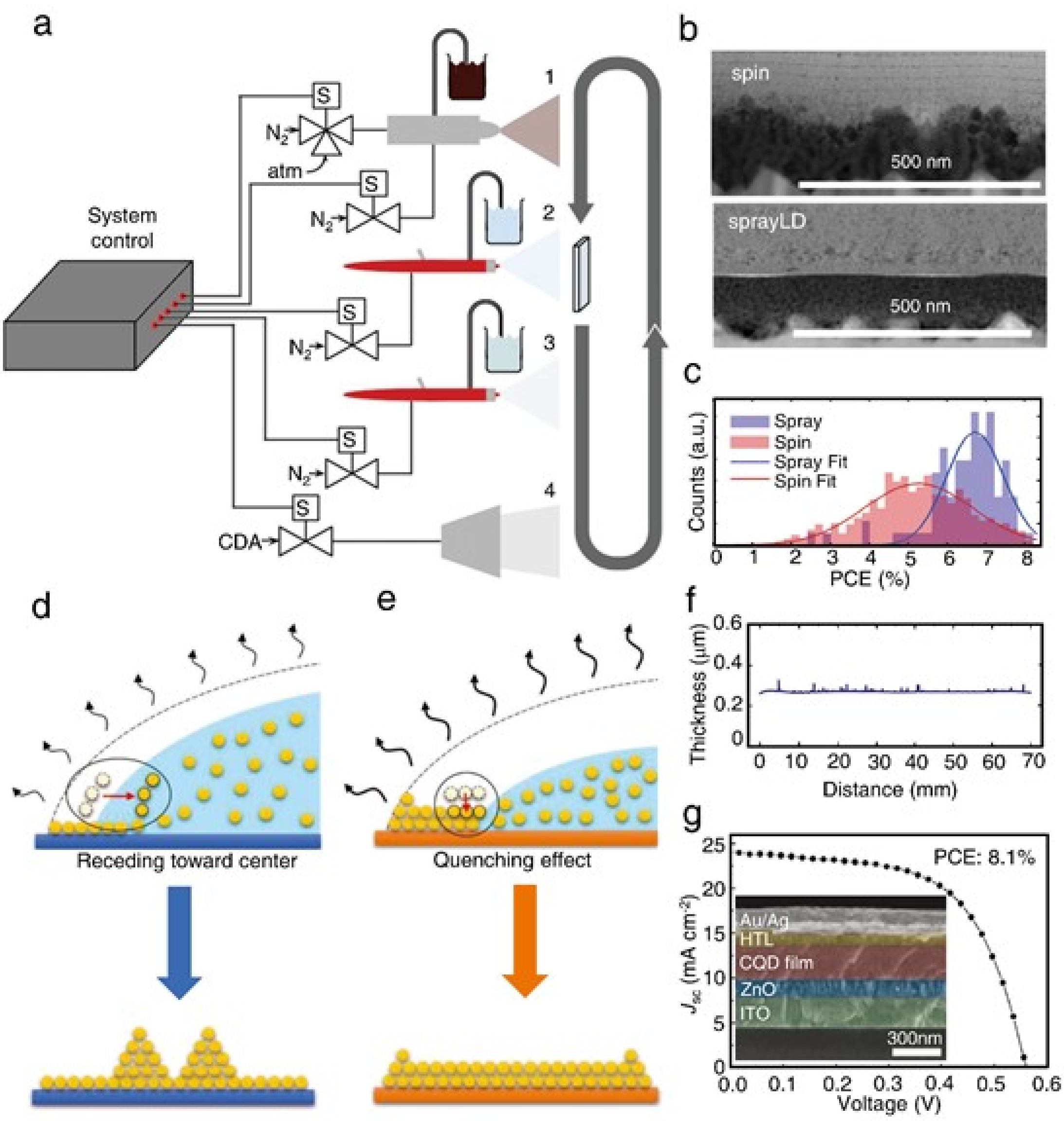

Figure 4. a) Schematic illustration of spray coating process. b) Focused ion beam transmission electron microscopy of spin-coated and sprayLD PbS QD films. c) Histograms showing a comparison between the efficiency for PbS QDSCs fabricated utilizing spin coating and sprayLD processes. d-e) Schematic of solute CQD redistribution when the solvent evaporation rate is slow (d) and fast (e) during the spray coating process. The dashed line represents an initial profile of droplet and the red arrow shows the position change of CQDs. f) Thickness

profile of CQD films on the glass substrate. g) *J–V* curves of the PbS QDSCs made by single-step spray-coated QD films. Inset image is a cross-sectional SEM image of the device. a-c) Reproduced with permission.[64] Copyright 2014, Wiley-VCH. d-g) Reproduced with permission.[51c] Copyright 2019, Wiley-VCH.

The spray-coating process, in general, has four stages: (i) generation of the ink-droplets, (ii) transportation of the droplets onto the substrate, (iii) the droplets coalescing into a wet film, and (iv) thin-film drying.[65] For CQD deposition using spray coating, the ligand-capped QD solution passes through a nozzle and is sheared into micron-sized droplets by an orifice or ultrasonic apparatus. After that, the generated droplets are directed to the substrate by a gas jet, wetting the surface of the substrate. Once a continuous wet film has been obtained, the nozzle is moved away and the carrier solvents start to evaporate, leaving a solid QD film. During the spray coating, the capacity of the droplets to merge together into a wet film is strongly associated with ink surface tension, nature of the substrate, the colloidal solution density, droplet diameter, viscosity, velocity, *etc*. Additionally, the QD solution concentration, the nature of the solvent for dispersing CQDs, substrate temperature, spray-head height/speed, and fluid flow rate should also be optimized to minimize “pooling” and de-wetting during solvent evaporation. The thickness of one spray coating step is mainly dependent on the concentration of the QD solution and the spraying time, while the thickness of the final QD film is controlled by the number of spray coating cycles.

Initially, spray coating was used to fabricate solar cells out of colloidal nanocrystals of $CuInSe_2$[66] and CdTe[67] with PCEs approaching 2% and 3%, respectively (well below the performance of their spin coated counterparts). Researchers soon began exploring direct translation of existing spin-coating methods for lab-scale PbS CQDs solar cell to spray coating method for large-area fabrication. Sung-Yeon Jang et al. fabricated PbS CQDs solar cell with a PCE of 4% by optimizing the fabrication conditions such as the spraying pressure, types of ligands, and duration of the ligand exchange in the solid state.[31b] Unfortunately, spray coating resulted in a substantial reduction in the performance of QDSCs as compared to those fabricated via spin coating. Sargent et al. investigated the origin of this performance loss and reported that insulating long-chain organic ligands on CQDs could accumulate in the film during the spray coating process, hindering the charge transport in the vertical direction for the resulting solid QD films.[64] To solve this issue, they developed a spray coating technique for PbS CQDs they named "sprayLD" (Figure 4a). This method is a fully automated process with near monolayer control and is analogous to atomic layer deposition (ALD). The sprayLD QD film is stripe free while the spin coated film presents a clear striping effect, suggesting the formation of voids as displayed in Figure 4b. This sprayLD approach produced high-quality QDSCs with a record PCE of 8.1%, even higher than that of the spin-cast counterparts as shown in Figure 4c.[64] The versatility of the sprayLD method for CQDs was further investigated by fabricating PV devices on various substrates including spherical lens substrates and one-axis-bended substrates for scaling up the manufacturing process. Meanwhile, the potential for transferring the spray-coating technique to roll-to-roll manufacturing was demonstrated by spray-coating the CQDs onto six substrates that were mounted on a rapidly rotating drum, achieving PbS QD solar cells with an average PCE of 6.7%.[68] To minimize the cost of the QD spray coating process, a supersonic spraying technique with facilitated solvent evaporation and non-compulsory post-deposition annealing procedure, was developed by Choi, et al. This technique achieved high-quality photovoltaic PbS QD films in 1 minute and minimized the amount of ink to <5mg for a 300-nm-thick QD layer on a 2.5×2.5 cm^2 substrate.[69] Recently, an ultrasonic spray coating system was used to tune the solute-redistribution dynamics of PbS CQD droplets by optimizing the movement of the contact line and the evaporation kinetics of the solvent as illustrated in Figure 4d-e. QDSCs with a smooth QD film and a notably large area of 100 cm^2 possess a remarkable PCE of 8.10% for PbS CQD solar cells (Figure 4f-g).[51c] Beyond the traditional lead chalcogenide based QDSCs, spray coating has also been effectively applied to the most recent colloidal PQDs. For $CsPbI_3$ PQDs, spray coating was employed by Tian et al. with an ultrathin-film purification process that was used to remove the residual long-chain organic ligands within the solid QD film. This method helped to improve the adhesive force between the PQDs and the substrate. A competitive efficiency of 11.2% was reported for the resulting $CsPbI_3$ perovskite QDSCs.[70]

Significant progress has been made in developing spray coating techniques for the fabrication of QDSCs. Such techniques however still bear the challenge of removing insulating ligands and optimizing the process parameters to create uniform and compact solid QD films. For instance, the droplet size and the droplet deposition distribution on the substrate surface are the most influential factors in the spraying process, but are not completely controllable.

Thus, multiple overlapping droplets over the entire substrate (which is essential for depositing a continuous film) cannot be achieved. Rather, multiple overlapping droplets can be observed only in patches in certain areas of the substrate. This is problematic since the surface tension on the overlapping droplets pulls the impacting droplets towards those already on the substrate. This leads to strikingly non-uniform morphologies and insulting organic ligand aggregation. These challenges still need to be solved, suggesting that there is ample scope in development of spray coating for QDSCs.

2.4 Inkjet Printing

Inkjet printing is another droplet-based method similar to spray coating with a series of advantages, such as efficient use of materials, contactless deposition, and high scalability. In addition, it has the unique advantage of high resolution, low-cost and mask-less patterning.[71]

In inkjet printing, the pressure inside the jet chamber is applied to eject an ink droplet from the nozzle to a precise position on substrates. Two representative inkjet printing methods for CQD solar cell are shown in Figure 5a-b.[72] A successful droplet formation requires the kinetic energy transferred from the piezoelectric transducer to the CQD ink to be large enough to overcome the surface tension at the nozzle. A volumetric change in the fluid is induced by an excitation pulse with the constructive and destructive interference traveling through the printhead. The printing resolution on the substrate mainly depends on the diameter of the orifice, the wettability of the substrate surface and the precision of the positioning control system. Based on the specification window of the printhead (Figure 5c),[72,73] the printability of the ink formulation relies on rheological ink properties such as density, viscosity, surface tension and the nozzle diameter. The nozzle and the substrate simultaneously move in relative motion according to a preset trajectory, so that the CQD ink can be evenly and precisely covered to the accurate position on substrates producing the desired patterns and structures.[71b] In addition, the deposition of a large-area film can also be performed quickly by using multiple nozzle heads covering the entire substrate. These characteristics of inkjet printing almost perfectly meet the needs of full color, light emitting diodes (LEDs). For example, a complicated pattern of the light-emitting layer can be seen in Figure 5d, and, to date, most studies on inkjet-printed CQD optoelectronic devices have focused on LEDs rather than solar cells.[74]

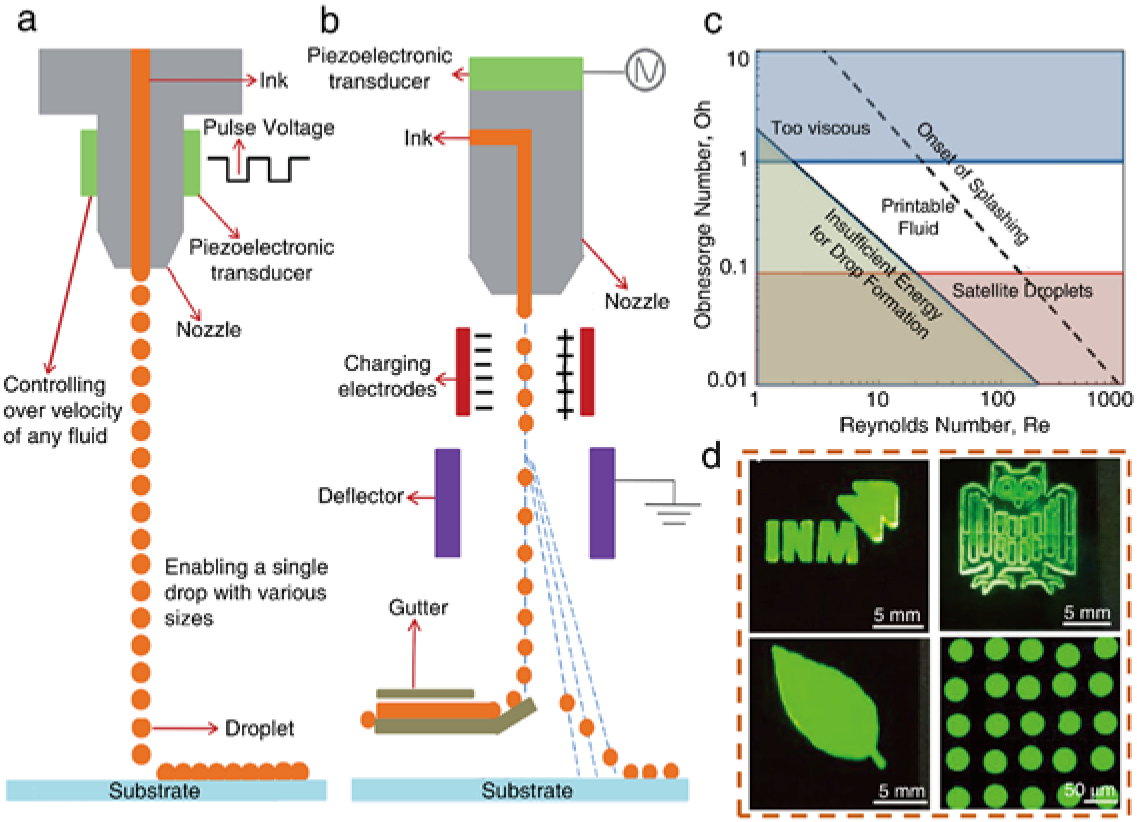

Figure 5. a) Schematic of the continuous inkjet printing process. b) Schematic of the "drop-on-demand" inkjet printing process. c) A plot showing properties of fluid that is suitable for inkjet printing process. d) Photographs of printed patterns and micrographs of the emitting pixels showing the versatility of inkjet printing. a-b) Reproduced with permission.[72] Copyright 2013, Royal Society of Chemistry. c) Reproduced with permission.[75] Copyright 2011, AIP publishing. d) Reproduced under the terms of Creative Commons CC BY license.[74a]

The limitations on quality of inkjet-printed CQDs films are mainly the results of nonuniform droplet formation, wetting, and drying. Many efforts have been made to optimize the CQD ink formulation to overcome these limitations, such as the use of mixed solvent systems that help tune the ejected droplet size, ensure wetting, and promote Marangoni flows that prevent coffee stain rings.[74a,76] Furthermore, using a dual ionic passivation of CQDs using zinc oleate ($Zn(OA)_2$) in a liquid phase ligand exchange, has been shown to solve the problems of low efficiency and fast degradation of devices from the inkjet printing process.[74c] Currently, inkjet-printed LEDs have been successfully commercialized and the research progress on inkjet printing for CQD LEDs suggests that it is feasible for the large area fabrication of QDSCs as well.

2.5 Blade Coating

In addition to the droplet-based methods discussed above, blade coating is a liquid-film based method, useful for continuous and large area film deposition. In blade coating, the ink is placed on a substrate and subsequently spread over the whole area by a blade, to form a thin film through the constant relative movement between the blade and the substrate. As compared to the droplet-based methods, blade coating can produce films from solutions with a wider range of viscosities and is inexpensive to set up. In addition, it enables quick and efficient formation of uniform thin films over large surface areas. With the ability to deposit on a range of rigid or flexible substrates without a large amount of solution waste. The thickness of blade coated films can be controlled by adjusting different deposition parameters like substrate speed and the height of the blade above the substrate.

In doctor-blade coating, as can be seen in Figure 6a, a sharp blade or knife is placed at a fixed distance (typically 10–500 mm) from the substrate surface and spreads the ink uniformly across the entire length of the substrate. The CQD ink travels along an inlet duct that drives the QD dispersion from an ideally stirred reservoir to a region of the substrate.[77] Shown schematically in Figure 6b, as the substrate moves, the solvent in the CQD ink evaporates within the liquid meniscus to form a saturated solution and densely packed QD array (wet film) that is transported from the deposition region by the moving substrate without disruption to the QD film. Then a continuous dry QD film is produced after the solvent in the wet film completely evaporates. The doctor-blade can operate at speeds of up to several meters per minute and achieve a very wide range of wet film thicknesses from twenty to several hundred microns. The thickness of the coat is not only defined by the distance between the blade and the substrate, but also dependent on the type of substrate, type and form of the blades, angle and position of the blade, viscosity of the paste, and speed of the base. The final thickness of the dry film, *d*, can be calculated from the empirical relationship:[79]

$$d = \frac{1}{2}\left(g\,\frac{c}{\rho}\right) \qquad (3)$$

where g is the gap distance between the blade and the substrate in cm, c is the concentration of the solid material in the ink in g/cm^3, and ρ is the density of the material in the final film in g/cm^3.

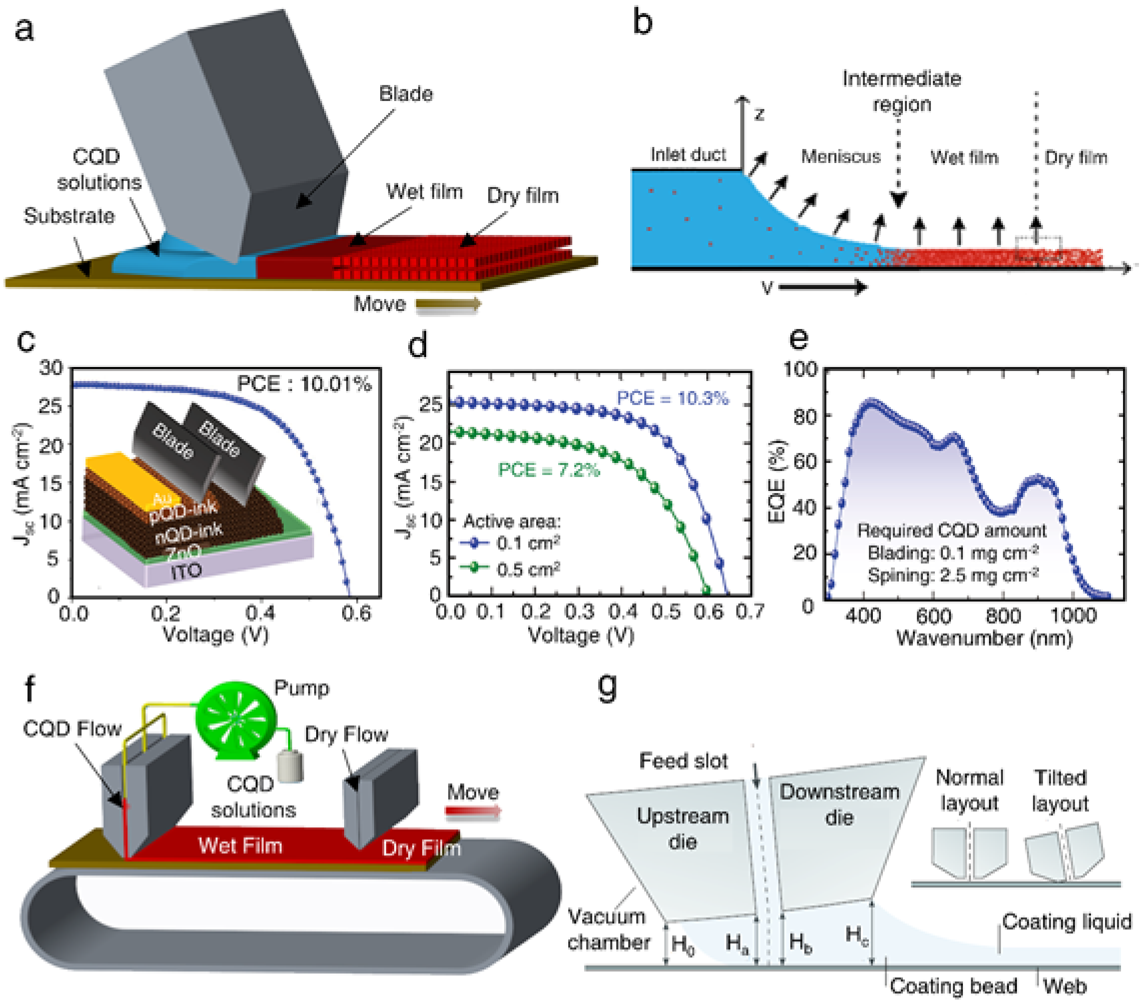

Figure 6. a) Schematic drawings of the blade coating process. b) Schematic of the CQD flow coating behavior. c) J–V curve of the PbS QDSC fabricated by successively blade coating p-type QD and n-type QD layers; the device structure is shown in the inset. d) J–V curves of 0.1 cm^2 (blue) and 0.5 cm^2 (green) active area blade coated PbS QDSCs by an oxygen-doping strategy. e) EQE spectrum of the 0.1 cm^2 blade coated solar cell in (c) with the comparison of the required QD amount between spin and blade coating. f) Schematic drawings of the slot-die coating process. g) Schematic illustration of a typical slot-die coating behavior. b) Reproduced with permission.[77] Copyright 2016, American Chemical Society. c) Reproduced with permission.[51a] Copyright 2008, Royal Society of Chemistry. d-e) Reproduced with

permission.[51b] Copyright 2018, Wiley-VCH. g) Reproduced with permission.[78] Copyright 2015, Wiley-VCH.

Despite blade coating being an easily implementable prototype tool for continuous deposition process, direct translation from well-established small-scale processes to blade coating still faces a number of physical and chemical challenges. Particularly, blade coating is not very effective when the CQDs deposition is accompanied with solid-state ligand exchange. This is because the exchange solutions containing short-chain ligands have a finite penetration depth. As a result, there is a limit to the QD film thickness that can be achieved with a single-step deposition. Thus, it is difficult to produce high quality QD films with nanoscale uniformity using single-step deposition technique like doctor blading. However, a CQD ink generated from liquid-phase ligand exchange can be quite effective in blade coating techniques. A variety of small molecule or atomic ligands like chalcogenidometallate complexes, chalcogenides, halides, pseudohalides, and halometallates have been explored for such processes.[40d,80] Halides and halometallates have shown the best prospects for solar cell applications due to excellent electronic passivation of the QD surface. Furthermore, n–p quantum junctions can be achieved by successively depositing an n-type QD ink and then a p-type QD ink, this also helps to overcome the thickness limit in blade coating methods. For example, n-type PbS QD ink can be prepared by the phase-transfer-exchange method using PbI_2 as the exchanging ligand, and p-type PbS QD ink can be produced by capping 3-mercaptopropionic acid (MPA) on PbS CQDs.[51a] As shown in Figure 6c, such CQDs can be deposited using blade coating to fabricate n–p quantum junction QDSC with a PCE of 10.01% that is comparable to their spin-coated counterparts.[51a] In another example of blade coating, Aram et al. demonstrated high-speed blade coating to fabricate PbS QDSC at ambient conditions irrespective of seasonal humidity variations (Figure 6d-e). For this purpose, they designed a simple oxygen-doping step and the QDSCs were fabricated under ambient conditions with 50–65% RH. The performance of these devices is very similar to those fabricated using spin coating, and this reported method shows an added advantage of requiring much smaller amounts of CQD material (0.1 mg cm^{-2} for blade coating vs 2.5 mg cm^{-2} for spin coating). Such improvements are bringing the QDSCs a significant step closer to industrial implementation.[51b] Nevertheless, there is still a long way to go in terms of optimizing the blade coating parameters: controlling the fabrication conditions and solvent engineering of the CQD ink in order to achieve high-quality blade-coated QD films. It must also be noted that contamination is a critical issue for the blade coating system, which cause serious streaks when the blade crosses over the substrate, impacting the film uniformity. Additionally, the shearing rate of the CQD solution is challenging to precisely control and plays a vital role in the thickness of the final QD film, which may lead to poor reproducibility of blade coating.[81]

2.6 Slot-die coating

Slot-die coating is another liquid-film based method for large-area processing which is very similar in design and principle to blade coating.[28b] This technique also uses a moving meniscus liquid edge of the precursor ink to drive the spread of the liquid film across the substrate as depicted in Figure 6f. The main difference is that in slot-die coating, the ink leaks out from a reservoir through a thin slit in the blade itself, with a linked pump for continuous production, and thus the wet film thickness is determined by the rate of ink deposited. A slot-die coater is generally composed of a slot-die head with an upstream die (or lip) and a downstream die.[78,82] In a typical process, the ink is injected into the slot-die head through a feed slot to form an upstream and a downstream meniscus in the coating bead, as liquid bridges between the head and the substrate (Figure 6g). When moving the substrate continuously, the wet film is deposited and then dried by heat or air flow. The quality of the resulting film is influenced by a set of operating parameters such as vacuum pressure applied in the coating bead, liquid viscosity, and surface tension. Moreover, slot-die coating is generally regarded as a pre-metered coating technique, in which the final film thickness can be precisely controlled based on the flow of the inks through the slit and the speed of the substrate. This makes the theoretical determination of wet-film thickness in slot-die coating more reliable when comparing to other coating methods. Also, it has shown by the Monte Carlo cost simulation model that slot-die coating is a scalable and industry-compatible coating technique, preferable over other roll-to-roll compatible techniques, due to the excellent processing window. Therefore, slot-die coating is of great interest for researchers who are working on translating thin-film fabrication from lab scale to commercial levels.[28b] Slot-die coating has been well studied in the field of PVs and is utilized to deposit light absorbing layers – like organic materials and perovskite inks – as well as the charge transport layers in device stacks.[83] Although slot-die coating has striking similarities with blade coating (which has already shown promise in QDSC fabrication) it has not been tried for CQDs so far. However, a recent publication showed the fabrication of $Cs_{0.16}FA_{0.84}Pb(I_{0.88}Br_{0.12})_3$ perovskite thin film solar cells using slot-die coating over an area of 100 cm^2.[84] From this example, we can confidently predict that slot-die coating exhibits promising prospects for the fabrication of large-area and flexible QDSCs.

Table 1. Comparison between different deposition techniques of QDs

Method	Cost	Scalability	Highest PCE achieved	Deposited film quality	Percentage of QD wastage	Deposition rate	Ref.
Spin Coating	Low	Low	High (16.6% for $CsPbI_3$)	High (controlled, uniform, reproducible)	High (>95%)	Very slow	35,61, 85
Drop Coating	Low	Low	Low (2.1% for PbS)	Low (uncontrolled, non-uniform, susceptible)	Low (<1%)	Medium	20a, 52,61
Dip Coating	Low	High	Middle (8.2% for PbSe)	Medium (uniform, susceptible, shrinkage)	Low (<1%)	Slow	60, 61,85a
Spray Coating	High	High	High (11.2% for $CsPbI_3$)	Low (uncontrolled, non-uniform)	Low (<1%)	Fast	61, 70, 74a
Inkjet Printing	Medium	High	-	Medium (controlled, non-uniform)	Low (<1%)	Fast	61, 74b, 74c
Blade Coating	Low	High	High (10.3% for PbS)	Medium (uniform, unreproducible, imprecise)	Medium (~35%)	Fast	51a, 61, 85a
Slot-die coating	High	High	-	High (controlled, uniform)	Low (~5%)	Fast	61, 85a, 86

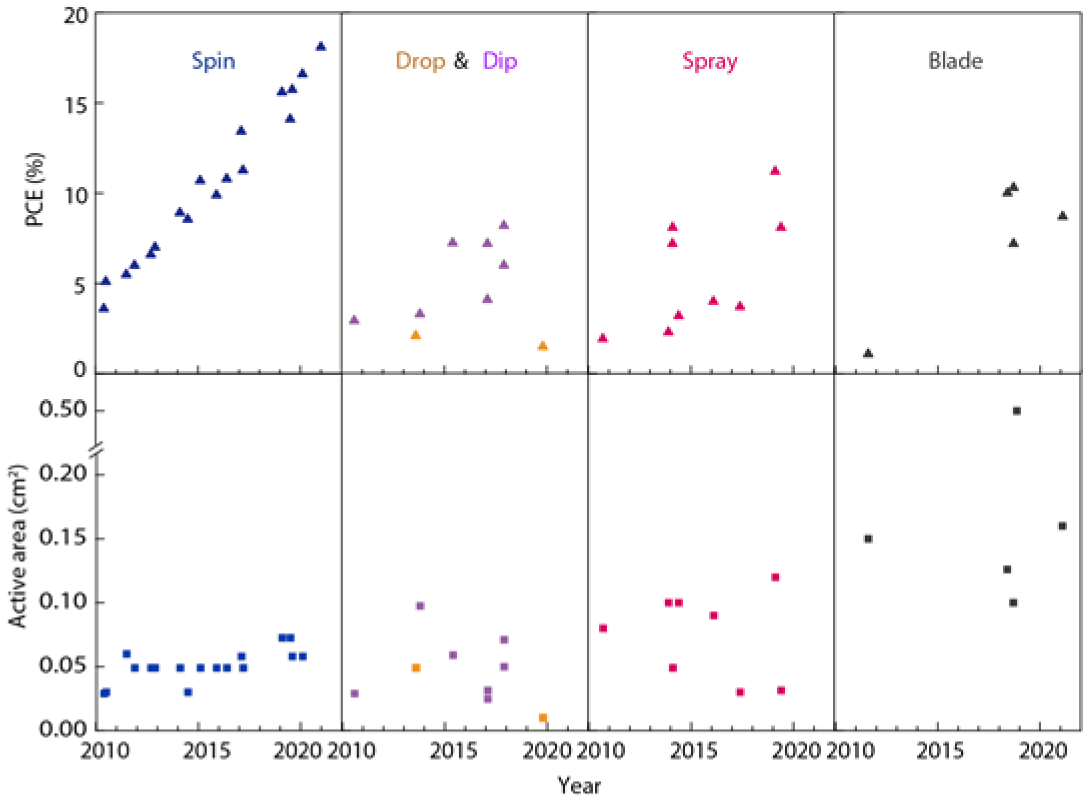

Figure 7. Comparison of all coating techniques for PV devices. Plot showing comparison of PCE and achieved active area in QDSCs fabricated using various deposition techniques since 2010. The data points are extracted from various reports discussed in this review.

Table 1 compares different QD deposition techniques employed during solar cell device fabrication and their effects on different aspects such as cost, scalability, highest PCE achieved, deposited film quality, percentage of material wastage and deposition rate. Furthermore, we summarize PCEs and active areas in QDSCs fabricated using different deposition techniques during the last decade (see Figure 7). As can be seen from this dataset, the efficiency and the active area in QDSCs are both significantly improved over time, except for spin coating where the active area stays tiny. It is evident that the majority of the efforts are being made to improve and optimize the QDSCs in research labs using spin coating, while drop and dip coating are rarely being studied in recent years. Attempts at large area fabrication of QDSCs are still in their infancy with only a few reports on spray coating and blade coating present in the literature. As discussed earlier, metal halide PQDs have recently taken the center stage of QDSC research, replacing the lead chalcogenide based materials as the PCE record-holding QD material. In the following section, we will shift the focus our discussion from general QD deposition techniques to perovskite QDSCs, as well as challenges and opportunities regarding their large-area fabrication.

3. Scale-up of PQD Solar Cells

3.1 Progress in PQD Solar Cells

Metal halide perovskite materials have attracted tremendous attention due to their high defect tolerance, high absorption coefficient and long photocarrier lifetime.[21b,87] These emerging perovskite semiconductors in CQD form offers the opportunity to achieve high efficiency PV devices. So far, materials scientists have shown enormous interest in PQDs as a new entrant to the QDSC technology landscape after their first successful synthesis by Schmidt et al. in 2014.[88] Controlled hot injection synthesis of all-inorganic monodisperse $CsPbX_3$ QDs (X = Cl, Br, I) was first demonstrated by Kovalenko et al. in 2015 with a high photoluminescence quantum yield (PLQY) of 90%.[9] Among the all-inorganic, $CsPbX_3$ QDs, $CsPbI_3$ is the best choice for a single-junction solar cell absorber material because the band gap is the smallest compared to using bromide or chloride. Interestingly, bulk $CsPbI_3$ in is not thermodynamically stable in the corner-sharing perovskite crystal phase in ambient conditions. The stability in this desired "black" perovskite phase of nanocrystalline $CsPbI_3$ has been attributed to the surface strain.[89] However, the chemical and structural instability of the $CsPbI_3$ PQDs in polar solvents (such as those typically used for solid-state ligand exchange in traditional lead chalcogenide based QDSCs) hindered their application in optoelectronic devices. Their application in QDSCs was realized only after Abhishek et al. demonstrated that the "magic" solvent methyl acetate (MeOAc) could remove the long-chain organic ligands without disturbing the chemical or structural integrity of the PQDs. The first perovskite QDSC was fabricated with the *n-i-p* structure displayed in Figure 8a, which showed a promising PCE of 10.77%.[90] Before going into the coating methods of PQDs and the challenges towards scale-up QDSC fabrication, we will quickly discuss different surface and interface engineering, and architecture design strategies employed so far in case of PQD solar cells, as understanding these strategies is important for developing and employing different coating techniques and scaling up.

The original ligand exchange process demonstrated by Abhishek et al. using MeOAc was later studied in detail by Wheeler et al., and it was proposed that MeOAc is hydrolyzed to acetic acid and methanol during the ligand exchange. Acetate ions can then replace the native oleate ligands on the QD surface.[91] Although removal of the oleate ligands helped achieve a high V_{oc}, the J_{sc} was still limited by carrier transport due to the remaining cationic ligands (oleylammonium) on the PQD surface, even after the MeOAc or NaOAc treatments.[90–92] To address this issue, Sanehira et al. carried out an additional step, treating the PQD solid films with a solution of MeOAc saturated with a variety of halide salts (AX). This treatment effectively replaced the long-chain surface oleylammonium ions with the smaller A^+ ions. Treating the QD film with FAI dramatically increased the carrier mobility of PQD film by more than a factor of two compared to the film using only MeOAc treatment, as shown in Figure 8b, leading to increased photocurrent and a certified QDSC efficiency of 13.43%.[29b] However, the processing window of the MeOAc and FAI treatments is very narrow and the ability to remove the original ligand is limited.[29b,91,93]

A variety of alternative surface treatments have been developed in order to improve the inter-dot electronic coupling, carrier transport, and overall PV performance.[94] To more efficiently remove the oleate ligands, Jigeon et al. further introduced a modification that involves treating the $CsPbI_3$ PQD films with a solution of sodium acetate (NaOAc) in MeOAc.[92] Unlike the neat MeOAc treatment, this NaOAc treatment contains OAc ions without the formation of the hydrolysis byproducts: methanol and proton. The efficient removal of surface oleate ligands leads to an improved photovoltaic performance with a PCE of 12.4%.[92] Recently, Ma et al. reported the use of short-chain secondary amines, specifically di-n-propylamine, to simultaneously remove the oleate and oleylammonium surface ligands, resulting a high PCE of ~15% for $CsPbI_3$ QDSCs.[40i]

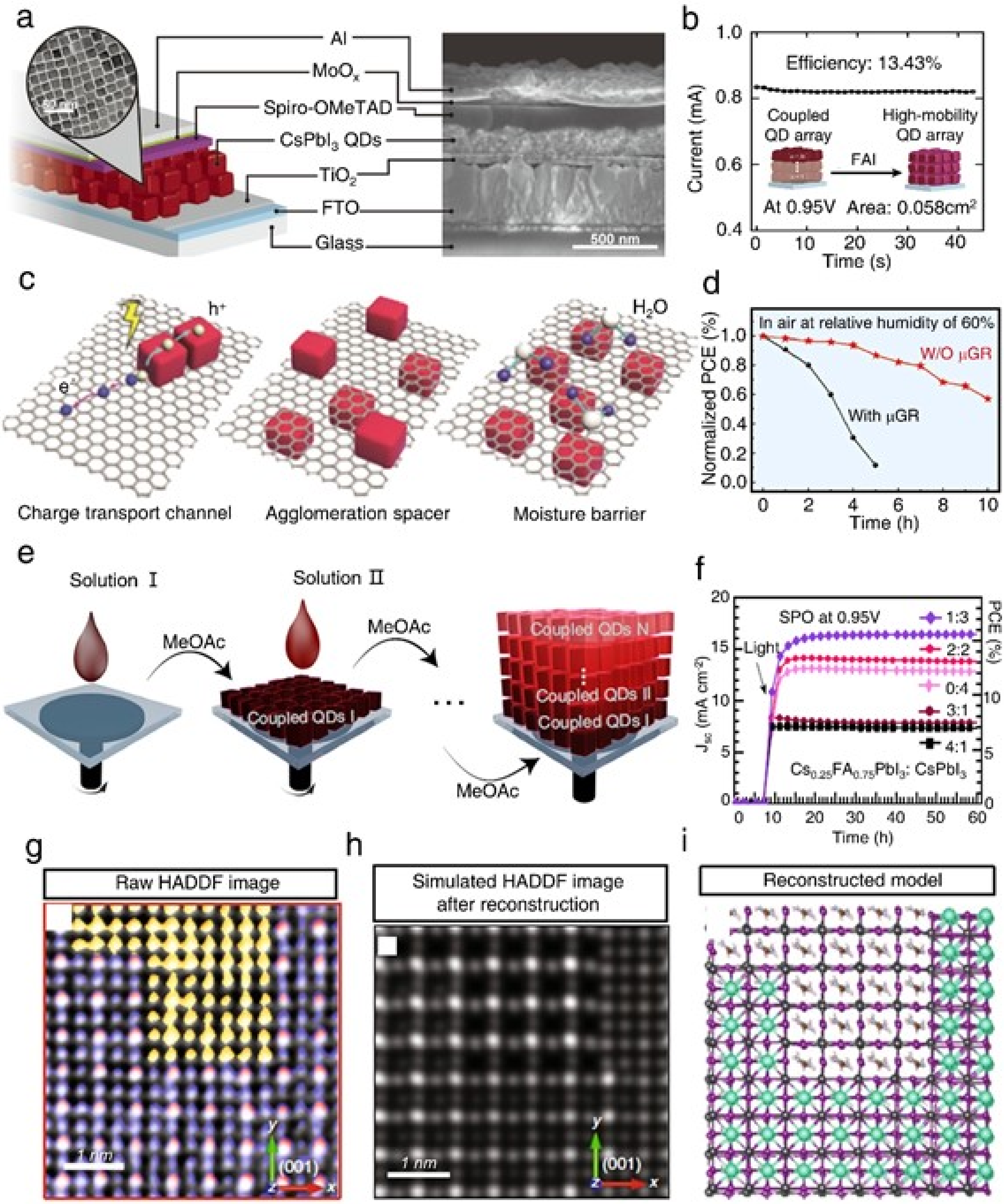

Figure 8. a) Schematic of a device stack with a TEM image of PQDs and a cross-sectional SEM image of the $CsPbI_3$ QDSC. b) Stabilized current at a constant voltage of 0.95 V for the $CsPbI_3$ QDSC. c) Schematic of the charge transport process and stabilization mechanism for μGR/$CsPbI_3$ QD film. d) Comparison of the stability for the $CsPbI_3$ and μGR/$CsPbI_3$ QDSCs in ambient with a relative humidity of ~60%. e) Schematic illustration of LBL assembly resulting in a PQD film composed of different layers of QDs. f) SPO at 0.95 V of QDSCs with different thicknesses of $Cs_{0.25}FA_{0.75}PbI_3$ and $CsPbI_3$ in the PQD absorber layer. g) The color-coded

atomic-resolution HAADF-STEM image of $Cs_{0.5}FA_{0.5}PbI_3$ QDs prepared using OA ligand-assisted cation-exchange strategy. The atom column with uniform and distinct contrast distribution are displayed as the yellow and the pink (blue) dots, respectively. h) The simulated atomic-resolution HAADF-STEM image of the $Cs_{0.5}FA_{0.5}PbI_3$ QDs after reconstruction. i) The atomic models for the original view of the $Cs_{0.5}FA_{0.5}PbI_3$ QDs along the [001] zone axis after reconstruction. a) Reproduced from references with permission.[90] Copyright 2016, American Association for the Advancement of Science. b) Reproduced under the terms of the Creative Commons Attribution-NonCommercial license.[29b] c-d) Reproduced with permission.[95] Copyright 2018, Wiley-VCH. e-f) Reproduced under the terms of Creative Commons CC BY license.[16] g-i) Reproduced with permission.[35] Copyright 2020, Nature Publishing Group.

Decreasing the number of defects within the PQD absorber layer is another distinct purpose of surface treatment. Ma et al. reported an efficient surface passivation strategy for $CsPbI_3$ PQDs using a variety of inorganic cesium salts (e.g., cesium acetate (CsAc)), which not only improves the intra-dot electronic coupling, but also fills vacancies at the $CsPbI_3$ QD surface.[96] This post-treatment process delivered an excellent efficiency of 14.10% for $CsPbI_3$ QDSCs. In addition, the surface defects of $CsPbI_3$ QDs can also be passivated by amino acids as dual-passivation ligands using a facile single-step ligand exchange strategy. For example, glycine ligands can significantly improve defect passivation in $CsPbI_3$ PQDs, resulting in QDSCs with an impressive PCE of 13.66%.[40f] In another example, a larger organic cation (as compared to Cs^+), guanidinium (GA^+), was added onto $CsPbI_3$ QD surfaces through ligand exchange, followed by a mild thermal annealing process that enhanced the carrier mobility up to 0.70 $cm^2 V^{-1} s^{-1}$,leading to a PCE of 15.21%.[23c] Table 2 lists a number of short-chain ligands that have been utilized for making highly efficient PQD devices. It can be seen from the table that the carboxylic acids (acetic, caproic, octanoic and benzoic acid), amines (propylamine, butylamine, hexylamine, octylamine and phenylamine) and their derivatives are typically used as surface capping ligands of PQDs. In addition, iodide and bromide salts have been proven advantageous for charge transport in active layer. These, therefore, allow us to speculate that the organic groups bearing lone pair electrons with moderate polarity could bind to under-coordinated A-site and B-site cations of PQDs (empty nonbonding surface orbitals)[97] by forming hydrogen bonds within the BX_6^{4-} framework (such as N-H-I-Pb) on PQD surfaces, while the addition of excess iodide and bromide ions are beneficial for filling the halide vacancies.[98]

Table 2. Summary of short-chain ligands employed in efficient PQD devices

PQD composition (X = Cl, Br, I)	Short-chain ligand	Device type	Ref.
$CsPbI_3$	Methyl acetate	Solar cell	90
$CsPbBr_3$	Methyl acetate, Ethyl acetate, Pacetate, Butyl acetate	Solar cell	99
$FAPbI_3$	Ethyl acetate, 2-pentanol, Acetonitrile,	Solar cell	100
$CsPbI_3$	Phenylammonium, Benzylammonium, Phenethylammonium	Solar cell	101
$CsSnX_3$	Trioctylphosphine oxide, Diethylenetriamine	Solar cell	102
$CsSn_{1-x}Pb_xI_3$	Tri-n-octylphosphine	Solar cell	103
$CsSnI_3$	Triphenylphosphite	Solar cell	104
$CsPbBrI_2$	Octylamine, Octanoic acid	Solar cell	105
CsPbI3	Adamantan-1-yl methanammonium	Solar cell	106
$CsPbI_3$	Octylamine, Octanoic acid, Dodecanoic acid, Dodecylamine, Caproic acid, Hexylamine, Acetic acid	Solar cell	107
$CsPbI_3$	N-propylamine, N-butylamine, N-hexylamine, N-octylamine, Phenylamine, Di-nethylamine, Di-n-butylamine, Di-n-octylamine, N-phenylaniline, Tri-n-propylamine	Solar cell	108
$CsPbI_3$	Phenyltrimethylammonium bromide	Solar cell	70
$CsPbI_3$	1,2-dichloroethane	Solar cell	109
$CsPbI_3$	Pyridine, Omercaptopyridine, P-mercaptopyridine	Solar cell	110
$CsPbI_3$	Guanidinium thiocyanate	Solar cell	111
$CsPbI_3$	Glycine, D-alanine, β-alanine, Lysine	Solar cell	112
$CsPbI_3$	tert-Butyl iodide and trioctylphosphine	Solar cell	113
$CsPbI_3$	L-phenylalanine	Solar cell, LED	114
$CsPbX_3$	4-Phenylbutylamine, Benzoic acid	LED	115
$CsPbBr_3$	Isopropylammonium bromide	LED	116
$CsPbBr_3$	Phenylmethylammonium bromide, Phenylethylammonium bromide, Phenylpropylammonium bromide, Phenylbutylammonium bromide	LED	117
$CsPbBr_3$	Dioctyldimethylammonium bromide, Didecyldimethyl ammonium bromide, Ditetradecyldimethyl ammonium bromide	LED	118
$CsPbBr_3$	N-propyltrimethoxysilane-dimethyloctadecylammonium bromine	LED	119
$CsPbX_3$	Di-dodecyl dimethyl ammonium bromide	LED	120

$CsPbI_3$	1-Octanethiol, 1-Dodecanethio, 1-Octadecanethiol	LED	121
$CsPbBr_3$	2-Aminoethanethiol	LED	122
$CsPbI_3$	Methyl acetate, Phenylethylamine, 2-(4-fluorophenyl)-ethylamine	LED	123
$CsPbBr_3$	Dido-decylamine, Phenethylamine	LED	124

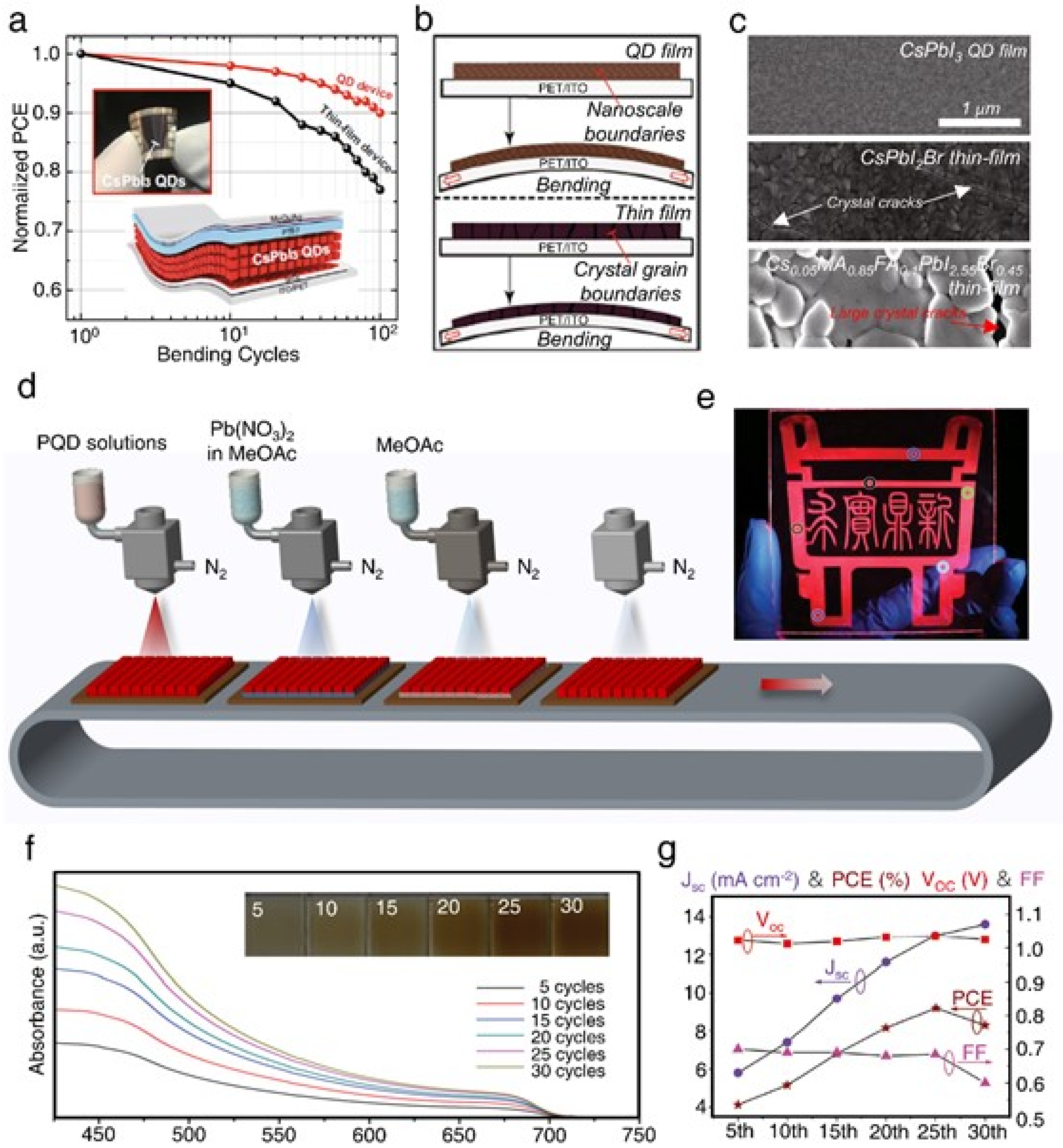

Figure 9. a) Normalized PCE of the flexible $CsPbI_3$ QDSC and a $CsPbI_2Br$ thin film solar cell as a function of bending cycles (inset: photograph of the flexible $CsPbI_3$ QDSC). b) Schematic of the bending mechanical testing of QD and thin films on a PET/ITO substrate. c) SEM images of the $CsPbI_3$ QD film, $CsPbI_2Br$, and mixed perovskite thin-film deposited on PET/ITO after the 1000-time mechanical bending test. d) Schematic drawings of the spray coating process

using an UFP method for PQDs. e) Photograph of spray-coated $CsPbI_3$ QD films on a 10 × 10 cm^2 substrate deposited in a complex pattern, shown under UV excitation. f) UV–Vis spectra and images (inset) of $CsPbI_3$ QD films with increasing cycles of spray coated layers by the UFP method. g) J_{sc}, V_{oc}, FF, and PCE for the spray coated $CsPbI_3$ QDSCs as a function of the deposition cycles by the UFP method. a-c) Reproduced under the terms of Creative Commons CC BY license.[125] e-g) Reproduced with permission.[70] Copyright 2019, Wiley-VCH.

In addition to the QD surface ligand engineering, other strategies have been attempted to improve the performance of $CsPbI_3$ QD solar cells. For example, μ-graphene (μGR) was used to crosslink $CsPbI_3$ PQDs to form a μ-graphene/$CsPbI_3$ film, demonstrated by Liu et al.[95] The resultant QD film provides not only an effective channel for carrier transport, but also dramatically improves their stability against moisture, humidity, and high temperature (Figure 8c-d). Interfacial engineering and surface engineering have also shown promise in improving the perovskite QDSCs. Ji et al. introduced a polymer–QD bulk heterojunction hybrid layer at the interface between PQD and HTL, which led to more efficient interfacial charge transfer with reduced carrier recombination loss, enhanced J_{sc}, and a PCE approaching 14%.[126]

Along with $CsPbI_3$ CQDs, the FA-containing PQDs like $FAPbI_3$ and $FA_{1-x}Cs_xPbI_3$ CQDs are also actively explored for solar cell applications. There have been fewer reports on organic/inorganic hybrid A-site perovskite QDSCs compared to the all-inorganic $CsPbX_3$ QDSCs since all-inorganic PQDs show much better photo and thermal stability and their synthesis and surface engineering are better optimized.[127] It is known in thin film halide perovskites that A-site alloying induces entropic stabilization of the perovskite structure under ambient conditions.[18,128] Moreover, tuning A-site compositions allows control over the band gap energy to some extents, paving the way for the development of ideal absorbers in a tandem solar cell architecture. $FAPbI_3$ is of interest to the solar cell community because of its slightly narrower band gap compared with $MAPbI_3$ and $CsPbI_3$, and its slower hot carrier cooling.[129] These advantageous properties inspire additional research into $FAPbI_3$ based QDSCs. Xue et al. demonstrated the first $FAPbI_3$ CQD based solar cell with an initial PCE of 8.38% by tailoring the polarity of the antisolvents for effective removal of the native insulating ligands.[130] This enhanced inter-dot electrical coupling while preserving the perovskite cores. Using similar methodology of the MeOAc/FAI treatment discussed above, $FAPbI_3$ QDSCs have reached a PCE of 9.01%.[18] Using a conjugated small molecule, like 2,2′-[[6,6,12,12-tetrakis(4-hexylphenyl)-6,12-dihydrodithieno[2,3-*d*:2′,3′-*d*′]-*s*-indaceno[1,2-*b*:5,6-*b*′]dithiophene-2,8-diyl]bis[methylidyne(3-oxo-1*H*-indene-2,1(3*H*)-diylidene)]]bis[propanedinitrile] (ITIC), which can promote effective charge separation, the established ITIC/$FAPbI_3$ CQD heterointerface enabled a remarkable PCE approaching 13% for $FAPbI_3$ QDSCs.[131] With the development of both $CsPbI_3$ and $FAPbI_3$ QDSCs, Hazarika et al. presented a post-synthetic cation-exchange approach for tunable A-site alloys of $Cs_{1-x}FA_xPbI_3$ PQDs spanning the complete compositional range (0<x<1),[18] which is difficult to achieve in corresponding thin films.[128,132] The QDSCs with these alloy compositions exhibited high V_{oc} with fewer losses than the thin-film perovskite devices of similar compositions or band gap. Zhao et al. demonstrated internal heterojunction solar cells by spin-coating two layers of $Cs_{1-x}FA_xPbI_3$ CQDs with different compositions, as displayed in Figure 8e.[16] This heterojunction facilitates charge separation at the internal interface, leading to improved photocarrier harvesting and resulting in a PCE with stabilized power output (SPO) of 15.74%, as illustrated in Figure 8f. In a very similar attempt, Li et al. demonstrated QDSCs with a $CsPbI_3$/$FAPbI_3$ QD bilayer heterojunction that resulted in 15.6% efficiency.[133] A certified efficiency of 16.6% for a QDSC was achieved using $Cs_{0.5}FA_{0.5}PbI_3$ QDs by Wang's group who utilized an oleic acid ligand-assisted cation-exchange strategy to synthesize high quality $Cs_{1-x}FA_xPbI_3$ PQDs, as shown in Figure 8g-i.[35]

The fast progress in the development in PQD synthesis, surface chemistry modification, and solar cell fabrication has raised the question of whether this PV technology can be scaled-up. Since this technology is still in its infancy, spin-coating has been the main deposition technique, which is the obvious choice for lab-scale device fabrication. Nonetheless, there are immense possibilities for scaling-up PQD PV technology. Yuan et al., very recently, reported the first flexible PQD solar cells on PET substrates with a record efficiency of 12.3%, and with higher mechanical endurance as compared to the thin-film perovskite solar cells, experimentally demonstrating the high roll-to-roll compatibility of PQD PVs (Figure 9a-c).[125] Here we summarize all the methods used to date for depositing PQD films in the fabrication of solar cells. As can be seen from Table 3, there is only one report from Tian's group who demonstrate the feasibility of spray coating PQDs for solar cell device fabrication. They developed a fully automated spray-coated technique using an ultrathin-film purification (UFP) method to successfully deposit high quality $CsPbI_3$ QD thin films for high-efficiency solar cells (see Figure 9d-g).[70] For the spray deposition process, the colloidal QD solution in octane is nebulized into very small droplets using a nozzle with high pressure N_2 gas. The droplets spray out from the nozzle and reach the substrate surface at high speed. In the UFP technology, each PQD layer is then treated by spray coating a $Pb(NO_3)_2$ in MeOAc solution. Finally, a high-pressure N_2 blade is utilized to dry residual solvent. To further increase charge carrier mobility and passivate the vacancy related defects, the PQDs films were treated with phenyl trimethyl ammonium bromide (PTABr) and the native oleylammonium ligands are partially substituted with phenyl trimethyl ammonium molecules. The final devices had an active area of 0.12 cm^2 and showed excellent stability with reasonably good PCE(>11%) after the optimization of the spray coating procedures (Figure 9f-g).[70] This is particularly interesting for the prospects of developing a fully automated industrial scale PQD solar fabrication process, allowing for continuous synthesis, QD deposition, and final module fabrication.[134]

The research on PQD solar cells is still in the developmental stage and the current focus is on improving device efficiency and stability by using highly controllable coating methods. It is known that for fabricating efficient PQD solar cells, the long-chain organic ligands in the solid films need to be replaced by small ligands during the deposition process. And the crystal phase stability of these PQD materials is extremely sensitive to their surface chemistry, particularly for all-inorganic PQDs. Hence, a well-controlled deposition process including careful ligand exchange can be recognized as one of the most essential ingredients for high performance PQD solar cells. Among all of the coating methods described in the manuscript, spin coating is one of the simplest methods that can enable highly uniform QD films, and also exhibits the highest degree of controllability and reproducibility (as shown in Table 1). To determine the best protocol for reproducibly fabricating the best device, using the common technique is the most efficient way at the current stage; rather than attempting to reduce the production cost or hastily scale up the device area using less explored techniques. Therefore, with the aim of improving device performance, in the current scenario, spin coating is the most widely employed technique that enables surface manipulation, chemical alloying, interfacial passivation etc. This may explain the continued reliance on spin coating to the near exclusion of all other coating methods as shown in Table 3. However, it should be noted that, compared to PQD-based solar cells, there are many reports of deposition techniques other than spin-coating for PbS/PbSe CQD-based solar cells, as demonstrated in Figure 7. The liquid phase ligand exchange process has been well-established for metal chalcogenide based CQDs, which allows the whole QD absorber layer to be produced by a single-step deposition using colloidal short-chain-ligand-capped QD inks without any requirement of post-ligand exchange.[40d,80] Thus, the applicability of more scalable coating methods, such as spray coating, blade coating, slot-die coating etc., will receive much attention once effective liquid-phase ligand exchange strategies are successfully implemented for PQDs. In addition, improving the tolerance of processing parameters for PQD films may be another way to develop scalable coating methods. It is not hard to imagine that after the significant breakthroughs in PQD solar cell performance and stability, a lot of effort will be focused on large scale PQD PV productions.

Table 3. Summary of reported coating techniques in PQD solar cell

Substrate/PQD absorber	Year	PCE	Active area	Depositing	Ref.
FTO/TiO_2/ $CsPbI_3$	2016	10.77	0.058	Spin coating	[90]
FTO/TiO_2/ $CsPbBr_3$	2016	5	0.0935	Spin coating	[135]
FTO/TiO_2/ $CsPbI_3$	2017	13.43	0.058	Spin coating	[29b]
ITO/TiO_2/ $CsPbBr_3$	2017	4.21	-	Spin coating	[136]
FTO/TiO_2/ $CsPbBrI_2$	2018	5.3	0.0314	Spin coating	[137]
FTO/TiO_2/ $CsPbI_3$	2018	8.83	0.058	Spin coating	[18]
FTO/TiO_2/ $FAPbI_3$	2018	12.37	0.058	Spin coating	[18]
FTO/TiO_2/ $CsPbBr_{1.5}I_{1.5}$	2018	7.94	0.06	Spin coating	[138]
FTO/TiO_2/ $CsPbI_3$	2018	12.55	0.0725	Spin coating	[21c]
FTO/TiO_2/ $CsPbI_3$	2018	11.41	0.09	Spin coating	[95]
ITO/SnO_2/ $FAPbI_3$	2018	8.38	0.1	Spin coating	[130]
FTO/TiO_2/ $CsPbI_3$	2018	8.1	0.11	Spin coating	[139]
ITO/PTAA/ $CsPbI_3$	2019	9.6	0.054	Spin coating	[140]
FTO/TiO_2/ $Cs_{0.25}FA_{0.75}PbI_3$/$CsPbI_3$	2019	15.74	0.058	Spin coating	[16]
FTO/TiO_2/ $FA_{1-x}Cs_xPb(I_{1-x}Br_x)_3$	2019	12.86	0.058	Spin coating	[21a]
FTO/TiO_2/ $CsPbI_3$	2019	13.12	0.0725	Spin coating	[127c]
FTO/TiO_2/ $CsPbI_3$	2019	13.3	0.0725	Spin coating	[92]
FTO/TiO_2/ $CsPbI_3$/$FAPbI_3$	2019	15.6	0.0725	Spin coating	[133]
FTO/TiO_2/ $CsPbI_3$	2019	14.1	0.0725	Spin coating	[96]

$FTO/TiO_2/CsPbI_3$	2019	11.2	0.12	Spray coating	[70]
$FTO/TiO_2/CsPbI_3$	2019	12.15	0.16	Spin coating	[127b]
$FTO/TiO_2/CsPbI_3$	2019	11.87	-	Spin coating	[127a]
$ITO/SnO_2/FAPbI_3$	2019	12.7	-	Spin coating	[131]
$ITO/ZnO/CsPbBr_3$	2019	2.43	-	Spin coating	[141]
$FTO/TiO_2/FAPbI_3$	2020	9	0.16	Spin coating	[142]
$ITO/NiO_x/FAPbI_3$	2020	5	0.16	Spin coating	[142]
$FTO/TiO_2/CsPbI_3/Cu_{12}Sb_4S_{13}$	2020	10.02	0.04	Spin coating	[143]
$FTO/NiO_x/CsPbI_3$	2020	13.1	0.056	Spin coating	[144]
$ITO/SnO_2/Cs_{1-x}FA_xPbI_3$	2020	16.6	0.058	Spin coating	[35]
$ITO/SnO_2/CsPbI_3$	2020	13.66	0.06	Spin coating	[40f]
$FTO/TiO_2/CsPbI_3$	2020	15.21	0.0725	Spin coating	[40f]
$FTO/TiO_2/CsPbI_3$	2020	14.9	0.0725	Spin coating	[40i]
$FTO/TiO_2/CsPbBr_3$	2020	5.01	0.0725	Spin coating	[106]
$FTO/TiO_2/CsPbI_3$	2020	13.8	0.0725	Spin coating	[126]
$FTO/TiO_2/FAPbI_3$	2020	13.2	0.0725	Spin coating	[126]
$FTO/c\text{-}TiO_2/m\text{-}TiO_2/CsPbI_3$	2020	14.32	0.09	Spin coating	[127e]
$FTO/TiO_2/CsPbI_3$	2020	14.62	0.0725	Spin coating	[145]
$FTO/TiO_2/CsPbI_3$	2020	14.03	0.059	Spin coating	[146]
$FTO/TiO_2/CsPbI_3$	2020	14.25	0.0725	Spin coating	[40g]
$FTO/TiO_2/CsPb_{1-x}Zn_xI_3$	2020	14.8	-	Spin coating	[127d]
$FTO/TiO_2/CsPbBr_3$	2020	4.23	0.096	Spin coating	[147]
$FTO/TiO_2/CsPbI_3$	2020	14.1	0.096	Spin coating	[40h]
$FTO/TiO_2/CsPbI_3$	2021	15.05	0.0725	Spin coating	[148]
$FTO/SnO_2/CsPbI_3/FAPbI_3$	2021	16.07	0.04	Spin coating	[149]
$FTO/SnO_2/CsPbI_3$	2021	14.5	0.096	Spin coating	[150]
$FTO/TiO_2/CsPbI_3$	2021	13.2	0.12	Spin coating	[33c]
$FTO/TiO_2/CsPbI_3$	2021	12.85	0.06	Spin coating	[93]
$FTO/TiO_2/CsPbI_3$	2021	15.1	0.096	Spin coating	[125]
$FTO/TiO_2/CsPbI_3$	2021	16.07	0.09	Spin coating	[151]
$FTO/TiO_2/CsPb_{0.965}Ag_{0.035}Br_{1.5}I_{1.5}$	2021	9.67	0.06	Spin coating	[152]
$FTO/TiO_2/CsPbBr_{1.5}I_{1.5}$	2021	8.07	0.06	Spin coating	[152]
$FTO/TiO_2/CsPbI_3$	2021	15.21	0.0725	Spin coating	[153]
$FTO/TiO_2/CsPbBr_{0.6}I_{2.4}$	2021	12.31	0.04	Spin coating	[154]
$FTO/TiO_2/CsPbI_3$	2021	13.5	-	Spin coating	[155]
$FTO/SnO_2/CsPbI_3$	2021	15.45	0.06	Spin coating	[113]

3.2 Challenges and Perspectives on Scaling up PQD PVs

In principle, there should not be any additional challenges for scaling up PQD PV technology when compared with the established lead chalcogenide based QD PVs.[22b,28b] The post-synthetic treatments, including ligand exchange, are similar in both material systems. There is one striking difference though: while lead chalcogenide QDs are compatible with many polar solvents like DMF, DMSO, ethanol, methanol, etc., PQDs have limited stability in such solvents. In the following section, as illustrated in Figure 10, we are briefly discussing some key issues that are crucial to address for scaling up PQD PV technology.

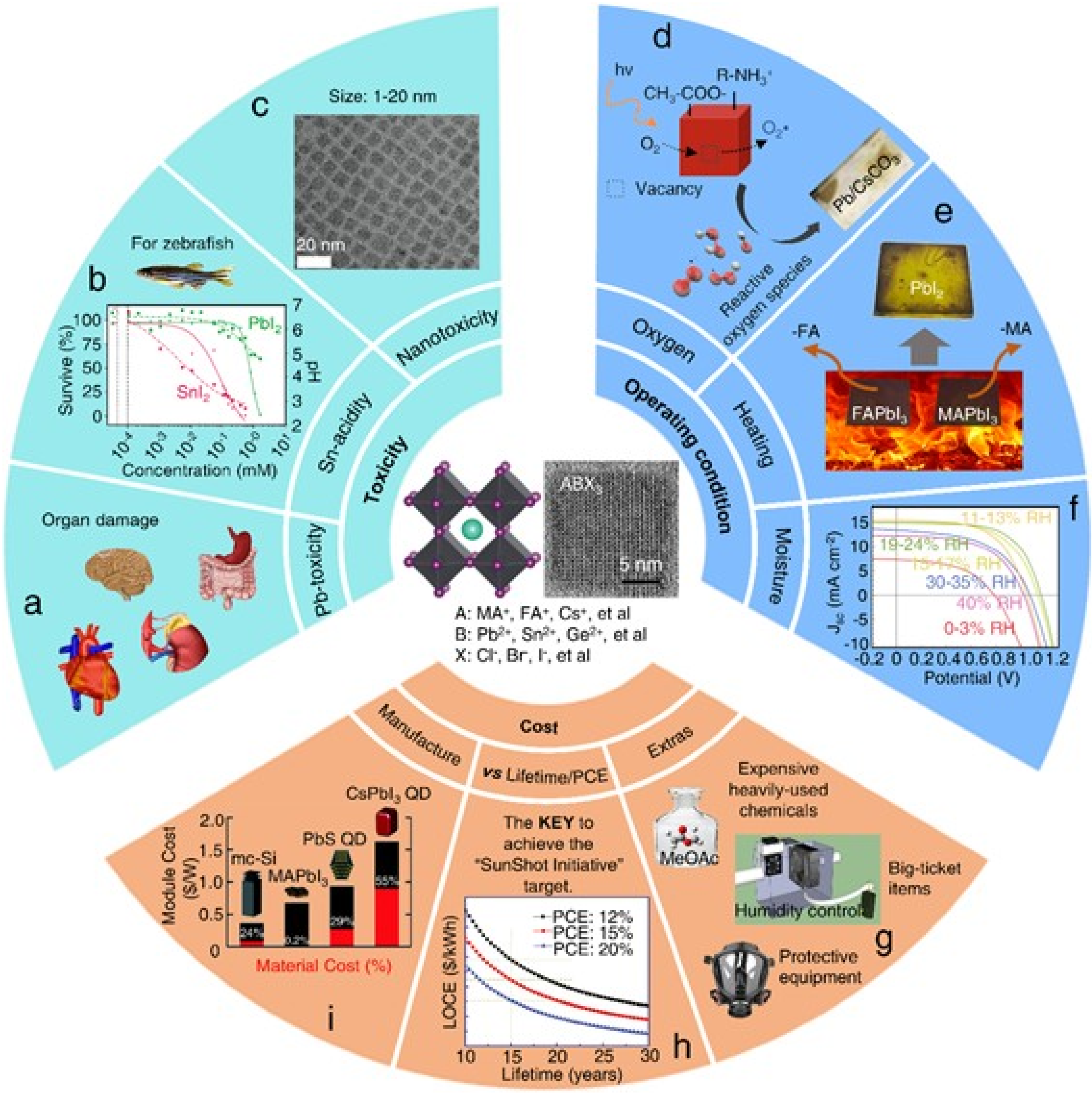

Figure 10. a) Demonstration of organ damage caused by Pb toxicity. b) The survival of zebrafish as a function of toxicant concentration and pH resulting from PbI_2 and SnI_2. c) TEM images of PQDs. d) Schematic drawings of $CsPbI_3$ QD photo-oxidation mechanism. e)

Illustrations of thermal degradation for $MAPbI_3$ and $FAPbI_3$ perovskites. f) *J*–*V* curves of $CsPbI_3$ QD devices fabricated at relative humidity levels ranging from 3 to 40%. g) Examples of additional costs in processing PQD PVs. h) The relationship between LCOE, PCE, and lifetime. i) Module cost breakdown for different absorbers assuming a 20% cell and 19% module efficiency. b) Reproduced under the terms of Creative Commons CC BY license.[156] d) Reproduced under the terms of Creative Commons CC BY license.[125] e) Reproduced with permission.[157] Copyright 2020, American Chemical Society. f) Reproduced with permission.[91] Copyright 2018, American Chemical Society. h) Reproduced under the terms of Creative Commons CC BY license.[28a] i) Reproduced under the terms of Creative Commons Attribution 3.0 Unported License.[158]

3.2.1 Toxicity

Pb is an essential element as the B-site cation in halide perovskites for state-of-the-art, high-performance perovskite PVs. For the most widely studied perovskite, $MAPbI_3$, the use of Pb is estimated at 38 mg per 1 kWh.[159] The presence of this heavy metal in PQD PV manufacturing, transportation, storage, and usage could cause serious threats to the environment and human health, particularly when pilot and industrial scale large-area fabrication is concerned. For instance, long-term exposure to lead, may cause blood disorders, anemia, abnormal activities of enzymes, etc.[160] Lead toxicity also commonly leads to behavioral problems, learning deficits and lowered IQ in children, as well as the damages to the digestive system, nervous system, respiratory system, reproductive system – both in adults and children.[161] The US Occupational Safety and Health Administration has clearly stated that the legal permissible exposure limit of lead in general industry is set to <0.05 mg/L.[162] Replacing the B-site Pb^{2+} in perovskite compositions (ABX_3) with relatively environmentally friendly elements, such as In^{1+} and Ga^{1+} from group III, Ge^{2+} and Sn^{2+} from group IV or Bi^{3+} and Sb^{3+} from group V of the periodic table[163] is generally considered to be a way to solve the Pb-toxicity problem.[164] Another way to discover possible Pb-free perovskite candidates is the introduction of an aliovalent metal cation leading to new perovskite chemical formulae like $AB'(I)B''(III)X_6$, $AB(V)X_6$, $A_2B(IV)X_6$ and $A_3B(III)_2X_9$.[159,165] For example, in 2015, Mitzi's group and Yan's group prepared a lead-free layered perovskite derivative, $Cs_3Sb_2I_9$, with a grain size of over 1 μm and a bandgap of 2.05 eV, showing potential for future developments in high-band gap PV applications.[163a] Moreover, incorporating nontoxic Bi^{3+} into the perovskite lattice to form double-perovskite structure of $Cs_2AgBiBr_6$ was reported by Slavney et al. and its room-temperature fundamental PL lifetime could reach ~660 ns, which is also encouraging for optoelectronics.[163b] In the past few years, colloidal lead-free PQDs have been intensively investigated following the development of their thin film counterparts, with the particular objective for use in efficient emitters and detectors.[166] For lead-free PQD solar cells, Wang et al. reported $CsSnI_3$ QDSCs with a PCE of 5.03% using an antioxidant solvent additive (triphenyl phosphate) to improve chemical stability.[104] Recently, Liu et al. found that highly luminescent Sn-based PQDs could be achieved *via* decreasing the density of tin vacancies though the trend in the chemical potential-dependent formation energies of various defects is opposite. They accordingly developed a colloidal synthesis strategy that leads to narrow-band-emissive $CsSnI_3$ QDs with a record photoluminescence quantum yield of 18.4%.[167] Nonetheless, these materials' optimization for solar cell applications will require significant work.

Furthermore, the potential hazards of acidification and nanotoxicity from scaling up PQD PVs must be evaluated. For example, Sn-based PQDs mentioned above are the most-researched candidates for lead-free perovskites, but there is the challenge of oxidation of Sn(II) to Sn(IV) in ambient or aqueous conditions, which leads to the formation of hydroiodic acid.[159] Biological experiments on zebrafish demonstrate that Sn^{2+} is more toxic to the ecosystem and could cause more severe acidification than Pb^{2+}.[156b] Additionally, nanoscale perovskite particles are known to be harmful to the liver, spleen, and lungs, as well as the circulatory, digestive, endocrine, immune and reproductive systems.[168] Adding in the exposure possibility of toxic elements from PQDs exacerbates the corresponding damage. In particular, when QD deposition involves spray coating, the PQD ink must be atomized into lots of very tiny droplets. These droplets can be dispersed in the air, polluting the environment, and inhaled by workers involved in the fabrication process. Therefore, developing nontoxic PQDs, along with establishing reliable health protection systems, is of utmost importance to the toxicity issue in PQD PV industrialization.

3.2.2 Deposition Operating Conditions

Another challenge for the large-area manufacturing of PQD films is that the deposition and ligand treatment of PQD films require tightly controlled environmental fabrication conditions including moisture, light, heat, and oxygen. Under the influence of these factors, metal halide perovskite materials may degrade *via* decomposition, hydration, oxidation, ion diffusion, polymorphic phase transformation, etc.[159] For instance, as recently reported by Luther's group, reactive oxygen species are responsible for the deprotonation of $CsPbI_3$ QD surface ligands, evolution of iodine, and the formation of metal carbonate species, resulting in the bleaching of $CsPbI_3$ PQD films.[169] Maintaining the native amine ligands or utilizing terminating bromide ligand salts can effectively reduce the surface under-coordinated sites to inhibit the photo-oxidation degradation reaction of $CsPbI_3$ PQDs. This degradation mechanism of PQDs is very different from their polycrystalline thin-film counterparts and the traditional chalcogenide-based CQDs. For the MA or FA containing organic–inorganic hybrid PQDs, the A-site organic species can diffuse out of the metal–halide octahedra structure and also are vulnerable to attack by H_2O because of the presence of the ammonium group.[170] Moreover, as mentioned earlier, the presence of moisture plays a crucial role in the ligand exchange process of PQDs since it involves hydrolysis of MeOAc to form acetic acid and methanol.[91] For effective ligand replacement and uniform film formation, the humidity of the environment needs to be strictly controlled between ~3%–30% in the deposition process.[91] It is generally observed that the PQD films exhibit uneven coverage when deposited at <3% relative humidity, and on the other hand, undergoes a change into yellow orthorhombic phase when the deposition is performed at >30% relative humidity. Hence, it is challenging to control the fabrication conditions required to produce high-quality PQD films on a large scale, while maintaining the stability in ambient conditions. A few attempts have been made to demonstrate unique approaches for the fabrication of environmentally stable $CsPbX_3$ PQD-based optoelectronic devices. For instance, $CsPbBr_3$ PQD/AlO_x nanocomposites can be prepared by using atomic layer deposition, which demonstrates exceptional stability towards exposure to air, irradiation, and heat.[171] Shi et al. utilized inorganic n-type and p-type materials as the carrier injectors and $CsPbBr_3$ PQD as the emissive layer to build an all-inorganic multilayer structure of an LED that showed excellent operational stability (75% of RH, 12 h) and maximum luminance of 6093.2 cd/m^2, along with an EQE of 3.79%.[172] Further, Shen's group demonstrated that $CsSn_{0.6}Pb_{0.4}I_3$ PQD films can have surprisingly high stability and their black phase could be retained even after one-month of storage in air.[103] These findings may open possibilities for ambient air-processed stable PQD solar cells in the near future. Along with these, fundamental research that focusses on understanding PQD degradation pathways should draw significant attention in the PV community, guiding the development of appropriate PQD manufacturing templates for industrialization of environmentally safe stable PQD PVs.

3.2.3 Cost

Low production cost with high performance is undoubtedly the major target in scaling up new PV technologies to compete with market-leading crystalline silicon and other established commercial PV technologies. To successfully industrialize PQD PVs, the costs involved in manufacturing, production equipment, materials, labor and other factors such as factory location, building, electricity, facility maintenance, etc, must be considered and estimated. In reality, except for the PQD material cost, the cost of manufacturing PQD PVs is quite similar to that of lead chalcogenide based QD PVs which has already been thoroughly analyzed for hot-injection synthesis.[173] Using Monte Carlo simulations, Jean et al. compared the cost of synthesizing PbS QDs with seven different reported synthetic methods and synthesizing $CsPbI_3$ QDs with the typical hot-injection method. According to their analysis, the median costs of PbS QDs are \$11 to \$59 per g and $CsPbI_3$ QD are \$73 per g.[158] Although the calculated costs in this report are not necessarily representative of a PQD solar cell factory because the materials used, processes, and equipment are still under development, it still suggests that the state-of-the-art PQD PVs with PCE <20% (~\$0.74 per W) has no competitive advantage in cost compared to silicon PVs (~\$0.20–0.40 per W).[174]

However, we find that if the module/device lifetime, which is one of the most sensitive factors for the cost of PVs, were improved to ~19 years with a current record device efficiency of 18.1%, or if the module efficiency could reach 22.3% with a lifetime of 15 years, the levelized cost of electricity (LCOE) is estimated to be \$0.06 per kWh using data drawn from previous reports,[28a,158] achieving the United States' "SunShot Initiative" goal.[175] Han's group stated that the LCOE for perovskite thin film solar cells with a module efficiency of 12% and a lifetime of 15 years is calculated to be \$0.035–0.049 per kWh, much lower than the cost of traditional energy sources (\$0.07–0.12 per kWh) reported in Levelized Cost and Levelized Avoided Cost of New Generation Resources in the Annual Energy Outlook,[28a,176] and they advocate for more efforts towards boosting the lifetime and efficiency of perovskite PVs, rather than identifying cheaper materials and procedures. Similarly, by enhancing the PCE and stability, the PQD PVs could have a huge potential to be competitive in the solar PV market as a lightweight and flexible alternative to conventional PV technology since there is no fundamental reason why PQDs must be expensive.[28b,159,177] But, it should be noted that the toxicity issues described above may cause an increase in the manufacturing costs due to resources needed for protecting factory workers' health during large-area fabrication. Precise control of the relative humidity, as is currently required for PQD processing, is expected to add extra cost during the fabrication process as well. Anhydrous MeOAc is an expensive chemical that bears the majority of the material cost of device fabrication, and unfortunately so far, no other alternative chemical has been found that can be used for post-synthetic chemical processing of the PQDs. Therefore, future work should aim at reducing the consumption of MeOAc, understanding cost barriers and drivers to establish low-cost manufacturing of PQDs with high-yield synthetic methods. To date there have been many reports where the material cost of PQDs have been reduced *via* increasing synthesis yield, enhancing process continuity and lowering reaction temperature. In particular, the introduction of di-*n*-propylamine can efficiently prevent the agglomeration of $CsPbI_3$ PQDs that occurs during MeOAc purification process, leading to the increased production yield by a factor of eight.[40i] Wang et al. reported a room-temperature synthesis of γ-phase $CsPbI_3$ PQDs by using 4-dodecylben-zenesulfonic acid as a ligand, which significantly reduced the energy consumption of PQD synthesis.[178] Recently, continuous flow synthetic strategies for halide PQDs have been successfully developed as a reliable synthesis technique, offering several advantages compared to batch processing approach, such as enhanced process intensification, high-throughput experimentation, and reduced reagent consumption.[98,134b,179] Such developments in PQD synthesis should reduce the material cost to a large extent. However, we still strongly believe that focusing efforts on overcoming performance and stability barriers of the QDSCs and modules would enable the commercialization of PQD PV technologies more quickly.

Different unique and logical approaches can be tried for improving the photoconversion efficiency of PQD PVs. For instance, three directions are worth pursuing for further improving the efficiency of PQD associated solar cells: building a PQD film with >1-μm thickness, exploring practical utilization based on unique intrinsic features of PQDs, and employing PQDs as passivators for reduction of the interfacial recombination between absorber and charge transport layer. Specifically, in the current generation of state-of-the-art PQD solar cells, the film thickness is limited (mostly <600 nm) due to a short carrier diffusion length. In such a case, 20%–40% of the incident photon flux is wasted, thus suppressing the J_{sc} of PV device.[139,180] So far, only a few studies address this issue in the case of PQD devices. For example, Yuan's group recently developed a P/N homojunction structure to overcome the thickness obstacle and demonstrated efficient PQD solar cells.[181] On the other hand, more fundamental studies and understanding are required to realize the potential of intrinsic features in PQDs to significantly enhance solar cell performance. For instance, multiple exciton generation (MEG) in CQDs can enable a dramatic increase of photogenerated carriers in the QD absorber by using surplus energy.[182] Besides, bulk perovskites have shown long-range hot-carrier transport and slow hot-carrier cooling lifetimes several orders of magnitude longer than conventional absorbers,[183] while PQDs exhibit around two orders of magnitude slower hot-carrier cooling times than their perovskite bulk counterparts and demonstrate an efficient, room temperature, hot-electron extraction up to ∼83%.[183a] In addition, Yb^{3+} doped $CsPbCl_3$ or $CsPb(Cl_{1-x}Br_x)_3$ PQDs demonstrated a remarkable PLQY approaching 200%, which is due to an efficient quantum cutting process where two emitted near-infrared photons can be generated from one absorbed visible photon.[184] Interestingly, very recent work by Gao and colleagues shows that $CsPbI_3$ PQDs exhibit the strongest carrier-longitudinal optical phonon interaction among all traditional semiconductors.[185] Lastly, it is known that the efficiency of the emerging perovskite solar cells is typically limited by the nonradiative recombination that occurs at the interface between absorber and charge transport layer.[186] However, Wieliczka et al. recently noticed that the interfaces between the PQD absorber and the charge transport layers have no significant impact on recombination losses, and the free charge carrier concentration of PQDs is orders of magnitude higher than that of perovskite thin films.[187] This not only explains why typical V_{oc} values in PQD based solar cells are higher compared to their bulk/thin film counterparts, but also further explains why the V_{oc} of bulk perovskite solar cells can be enhanced through inserting a PQD layer between perovskite thin-film layer and charge transport layer. Furthermore, the perovskite QD/bulk heterojunction can be established to enhance photogenerated carrier harvesting of perovskite absorber, and concurrently enables effective interfacial passivation. So, overall, we expect that finding ways to increase the J_{sc} is the way forward to enhance the PCE to be competitive to the bulk devices, as V_{oc} and FF are already better or comparable to that of their bulk counterparts.

4. Conclusions and Future Prospects

With the established CQD manufacturing industries and a good number of start-up companies like NanoSys, UbiQD, Avantama, Nanoco Technologies, Quantum Solutions LLC, working on large scale production of CQDs as well as on industrial scale application in some key areas, it will not be exaggerated to envision that commercial CQD-based solar modules may soon become a reality. The fast progress in materials development and understanding of their fundamental properties has raised this hope even more. In order to achieve industrial-scale use of QD PV, research must shift its focus to how the large area deposition techniques summarized here, such as spray coating, slot-die coating, and blade coating can be controllably employed. In parallel, the job at hand for the QD research community is to continue improving the single-junction device conversion efficiency >20% and find solutions to the fundamental challenges, like eliminating toxicity, enhancing QDSC stability, and replacing expensive chemicals used in device fabrication, especially for the emerging colloidal PQDs. By simultaneously addressing these obstacles to QDSC industrial production, we will be able to realize tremendous opportunities for single junction QDSCs, and combine them with other PV technologies for superior designs, such as QD/thin film perovskite tandem PV modules.

Acknowledgments

This work was supported by the China Postdoctoral Science Foundation (2020M680861) and the National Natural Science Foundation of China (52102266). AH gratefully acknowledge the support from the Department of Science and Technology-Science and Engineering Research Board (DST-SERB), Government of India (project no. SRG/2020/000258), and CSIR-Indian Institute of Chemical Technology, Hyderabad. This work was authored in part by the National Renewable Energy Laboratory, operated by Alliance for Sustainable Energy, LLC, for the U.S. Department of Energy (DOE) under Contract No. DE-AC36-08GO28308. J.M.L. and B.M.W. acknowledge support from the Center for Hybrid Organic Inorganic Semiconductors for Energy (CHOISE), an Energy Frontier Research Center funded by the Office of Science, Office of Basic Energy Sciences within the U.S. Department of Energy (DOE). The views expressed in the article do not necessarily represent the views of the DOE or the U.S. Government. Q. Z. and R. H. contributed equally to this work.

Conflict of Interest

The authors declare no conflict of interest.

Received: ((will be filled in by the editorial staff))
Revised: ((will be filled in by the editorial staff))
Published online: ((will be filled in by the editorial staff))

References

[1] National Renewable Energy Laboratory, Best Research-Cell Efficiency Chart, https://www.nrel.gov/pv/cell-efficiency.html, accessed: July, **2021**.

[2] Clean Energy Reviews, Most Efficient Solar Panels 2021, https://www.cleanenergyreviews.info/blog/most-efficient-solar-panels, accessed: July, **2021**.

[3] a) D. Li, D. Zhang, K.-S. Lim, Y. Hu, Y. Rong, A. Mei, N.-G. Park, H. Han, *Adv. Funct. Mater.* **2021**, *31*, 2008621; b) N. Rolston, A. Sleugh, J. P. Chen, O. Zhao, T. W. Colburn, A. C. Flick, R. H. Dauskardt, *Front. Energy Res.* **2021**, *9*, 5495.

[4] a) G. Kim, H. Min, K. S. Lee, D. Y. Lee, S. M. Yoon, S. I. Seok, *Science* **2020**, *370*, 108; b) H. Lu, Y. Liu, P. Ahlawat, A. Mishra, W. R. Tress, F. T. Eickemeyer, Y. Yang, F. Fu, Z. Wang, C. E. Avalos, B. I. Carlsen, A. Agarwalla, X. Zhang, X. Li, Y. Zhan, S. M. Zakeeruddin, L. Emsley, U. Rothlisberger, L. Zheng, A. Hagfeldt, M. Grätzel, *Science* **2020**, *370*, 74; c) J. Jeong, M. Kim, J. Seo, H. Lu, P. Ahlawat, A. Mishra, Y. Yang, M. A. Hope, F. T. Eickemeyer, M. Kim, Y. J. Yoon, I. W. Choi, B. P. Darwich, S. J. Choi, Y. Jo, J. H. Lee, B. Walker, S. M. Zakeeruddin, L. Emsley, U. Rothlisberger, A. Hagfeldt, D. S. Kim, M. Grätzel, J. Y. Kim, *Nature* **2021**, *592*, 381.

[5] Z. Song, C. L. McElvany, A. B. Phillips, I. Celik, P. W. Krantz, S. C. Watthage, G. K. Liyanage, D. Apul, M. J. Heben, *Energy Environ. Sci.* **2017**, *10*, 1297.

[6] T. Wu, Z. Qin, Y. Wang, Y. Wu, W. Chen, S. Zhang, M. Cai, S. Dai, J. Zhang, J. Liu, Z. Zhou, X. Liu, H. Segawa, H. Tan, Q. Tang, J. Fang, Y. Li, L. Ding, Z. Ning, Y. Qi, Y. Zhang, L. Han, *Nano-Micro Lett.* **2021**, *13*, 152.

[7] W. Stanislaw, Polish Firm Opens Cutting-Edge Solar Energy Plant, https://techxplore.com/news/2021-05-firm-cutting-edge-solar-energy.html, accessed: May, **2021**.

[8] a) W. U. Huynh, J. J. Dittmer, W. C. Libby, G. L. Whiting, A. P. Alivisatos, *Adv. Funct. Mater.* **2003**, *13*, 73; b) I. Gur, N. A. Fromer, M. L. Geier, A. P. Alivisatos, *Science* **2005**, *310*, 462; c) G. I. Koleilat, L. Levina, H. Shukla, S. H. Myrskog, S. Hinds, A. G. Pattantyus-Abraham, E. H. Sargent, *ACS Nano* **2008**, *2*, 833; d) K. W. Johnston, A. G. Pattantyus-Abraham, J. P. Clifford, S. H. Myrskog, D. D. MacNeil, L. Levina, E. H. Sargent, *Appl. Phys. Lett.* **2008**, *92*, 151115.

[9] L. Protesescu, S. Yakunin, M. I. Bodnarchuk, F. Krieg, R. Caputo, C. H. Hendon, R. X. Yang, A. Walsh, M. V. Kovalenko, *Nano Lett.* **2015**, *15*, 3692.

[10] R. Vidal, J.-A. Alberola-Borràs, S. N. Habisreutinger, J.-L. Gimeno-Molina, D. T. Moore, T. H. Schloemer, I. Mora-Seró, J. J. Berry, J. M. Luther, *Nat. Sustain.* **2021**, *4*, 277.

[11] M. R. Bergren, N. S. Makarov, K. Ramasamy, A. Jackson, R. Guglielmetti, H. McDaniel, *ACS Energy Lett.* **2018**, *3*, 520.

[12] a) K. Wu, H. Li, V. I. Klimov, *Nat. Photonics* **2018**, *12*, 105; b) F. Meinardi, F. Bruni, S. Brovelli, *Nat. Rev. Mater.* **2017**, *2*, 69.

[13] National Renewable Energy Laboratory, IN^2: Catalyst to Success, https://www.nrel.gov/innovate/assets/pdfs/in2-2020-annual-report.pdf, accessed: March, **2020**.

[14] A. James, Ubigro ‘Quantum Dot’ Nanomaterial Set to Boost Greenhouse Productivity, https://www.foodandfarmingtechnology.com/news/business/ubigro-quantum-dot-nanomaterial-set-to-boost-greenhouse-productivity.html, accessed: December, **2020**.

[15] a) PR Newswire, Optimizing Spectral Quality for Growing Plants on Space Missions Using Quantum Dot Films, https://apnews.com/press-release/pr-newswire/technology-entertainment-business-science-materials-industry-

4c424c48c2cbabd3527533422a262c3a, accessed: January, **2021**; b) T. S. Perry, Quantum Dots Shift Sunlight's Spectrum to Speed Plant Growth, https://spectrum.ieee.org/quantum-dots-shift-sunlights-spectrum-to-speed-plant-growth, accessed: June, **2020**; c) C. Bettenhausen, UbiQD and Nanosys Partner on Quantum Dots for Greenhouse Films, https://cen.acs.org/food/agriculture/UbiQD-Nanosys-partner-quantum-dots/98/i22, accessed: June, **2020**; d) UbiQD, UbiGro Luminescent Film Improving Cannabis Yield Through Spectral Modification, https://www.mmjdaily.com/article/9357750/ubiqd-ubigro-luminescent-film-improving-cannabis-yield-through-spectral-modification, accessed: September, **2021**.

[16] Q. Zhao, A. Hazarika, X. Chen, S. P. Harvey, B. W. Larson, G. R. Teeter, J. Liu, T. Song, C. Xiao, L. Shaw, M. Zhang, G. Li, M. C. Beard, J. M. Luther, *Nat. Commun.* **2019**, *10*, 2842.

[17] a) X. Wang, G. I. Koleilat, J. Tang, H. Liu, I. J. Kramer, R. Debnath, L. Brzozowski, D. A. R. Barkhouse, L. Levina, S. Hoogland, E. H. Sargent, *Nat. Photonics* **2011**, *5*, 480; b) L. Hu, Y. Wang, S. B. Shivarudraiah, J. Yuan, X. Guan, X. Geng, A. Younis, Y. Hu, S. Huang, T. Wu, J. E. Halpert, *ACS Appl. Mater. Inter.* **2020**, *12*, 2313; c) B. Chen, S.-W. Baek, Y. Hou, E. Aydin, M. de Bastiani, B. Scheffel, A. Proppe, Z. Huang, M. Wei, Y.-K. Wang, E.-H. Jung, T. G. Allen, E. van Kerschaver, F. P. García de Arquer, M. I. Saidaminov, S. Hoogland, S. de Wolf, E. H. Sargent, *Nat. Commun.* **2020**, *11*, 1257; d) A. Manekkathodi, B. Chen, J. Kim, S.-W. Baek, B. Scheffel, Y. Hou, O. Ouellette, M. I. Saidaminov, O. Voznyy, V. E. Madhavan, A. Belaidi, S. Ashhab, E. Sargent, *J. Mater. Chem. A* **2019**, *7*, 26020; e) Y. Gao, J. Zheng, W. Chen, L. Yuan, Z. L. Teh, J. Yang, X. Cui, G. Conibeer, R. Patterson, S. Huang, *J. Phys. Chem. Lett.* **2019**, *10*, 5729; f) H. I. Kim, S.-W. Baek, M.-J. Choi, B. Chen, O. Ouellette, K. Choi, B. Scheffel, H. Choi, M. Biondi, S. Hoogland, F. P. García de Arquer, T. Park, E. H. Sargent, *Adv. Mater.* **2020**, *32*, 2004657.

[18] A. Hazarika, Q. Zhao, E. A. Gaulding, J. A. Christians, B. Dou, A. R. Marshall, T. Moot, J. J. Berry, J. C. Johnson, J. M. Luther, *ACS Nano* **2018**, *12*, 10327.

[19] a) T. Leijtens, K. A. Bush, R. Prasanna, M. D. McGehee, *Nat. Energy* **2018**, *3*, 828; b) D. Zhao, Y. Yu, C. Wang, W. Liao, N. Shrestha, C. R. Grice, A. J. Cimaroli, L. Guan, R. J. Ellingson, K. Zhu, X. Zhao, R.-G. Xiong, Y. Yan, *Nat. Energy* **2017**, *2*, 151; c) J. Kromdijk, K. Głowacka, L. Leonelli, S. T. Gabilly, M. Iwai, K. K. Niyogi, S. P. Long, *Science* **2016**, *354*,

857; d) Z. Shi, J. Guo, Y. Chen, Q. Li, Y. Pan, H. Zhang, Y. Xia, W. Huang, *Adv. Mater.* **2017**, *29*, 1605005.

[20] a) A. Fischer, L. Rollny, J. Pan, G. H. Carey, S. M. Thon, S. Hoogland, O. Voznyy, D. Zhitomirsky, J. Y. Kim, O. M. Bakr, E. H. Sargent, *Adv. Mater.* **2013**, *25*, 5742; b) Z. Ning, H. Dong, Q. Zhang, O. Voznyy, E. H. Sargent, *ACS Nano* **2014**, *8*, 10321; c) H. Aqoma, N. Barange, I. Ryu, S. Yim, Y. R. Do, S. Cho, D.-H. Ko, S.-Y. Jang, *Adv. Funct. Mater.* **2015**, *25*, 6241; d) M. Liu, O. Voznyy, R. Sabatini, F. P. García de Arquer, R. Munir, A. H. Balawi, X. Lan, F. Fan, G. Walters, A. R. Kirmani, S. Hoogland, F. Laquai, A. Amassian, E. H. Sargent, *Nat. Mater.* **2017**, *16*, 258; e) J. Z. Fan, M. Liu, O. Voznyy, B. Sun, L. Levina, R. Quintero-Bermudez, M. Liu, O. Ouellette, F. P. García de Arquer, S. Hoogland, E. H. Sargent, *ACS Appl. Mater. Inter.* **2017**, *9*, 37536.

[21] a) M. Suri, A. Hazarika, B. W. Larson, Q. Zhao, M. Vallés-Pelarda, T. D. Siegler, M. K. Abney, A. J. Ferguson, B. A. Korgel, J. M. Luther, *ACS Energy Lett.* **2019**, *4*, 1954; b) J. Yuan, A. Hazarika, Q. Zhao, X. Ling, T. Moot, W. Ma, J. M. Luther, *Joule* **2020**, *4*, 1160; c) J. Yuan, X. Ling, Di Yang, F. Li, S. Zhou, J. Shi, Y. Qian, J. Hu, Y. Sun, Y. Yang, X. Gao, S. Duhm, Q. Zhang, W. Ma, *Joule* **2018**, *2*, 2450.

[22] a) A. R. Kirmani, J. M. Luther, M. Abolhasani, A. Amassian, *ACS Energy Lett.* **2020**, *5*, 3069; b) H. Lee, H.-J. Song, M. Shim, C. Lee, *Energy Environ. Sci.* **2020**, *13*, 404;

[23] a) R. Debnath, J. Tang, D. A. Barkhouse, X. Wang, A. G. Pattantyus-Abraham, L. Brzozowski, L. Levina, E. H. Sargent, *J. Am. Chem. Soc.* **2010**, *132*, 5952; b) D. A. R. Barkhouse, R. Debnath, I. J. Kramer, D. Zhitomirsky, A. G. Pattantyus-Abraham, L. Levina, L. Etgar, M. Grätzel, E. H. Sargent, *Adv. Mater.* **2011**, *23*, 3134; c) X. Ling, J. Yuan, X. Zhang, Y. Qian, S. M. Zakeeruddin, B. W. Larson, Q. Zhao, J. Shi, J. Yang, K. Ji, Y. Zhang, Y. Wang, C. Zhang, S. Duhm, J. M. Luther, M. Grätzel, W. Ma, *Adv. Mater.* **2020**, *32*, 2001906.

[24] a) G. Zhai, A. Bezryadina, A. J. Breeze, D. Zhang, G. B. Alers, S. A. Carter, *Appl. Phys. Lett.* **2011**, *99*, 63512; b) B. Martín-García, Y. Bi, M. Prato, D. Spirito, R. Krahne, G. Konstantatos, I. Moreels, *Sol. Energy Mater. Sol. Cells* **2018**, *183*, 1.

[25] H. Aqoma, M. Al Mubarok, W. T. Hadmojo, E.-H. Lee, T.-W. Kim, T. K. Ahn, S.-H. Oh, S.-Y. Jang, *Adv. Mater.* **2017**, *29,* 1605756.

[26] G. H. Carey, K. W. Chou, B. Yan, A. R. Kirmani, A. Amassian, E. H. Sargent, *MRS Commun.* **2013**, *3*, 83.

[27] M. Law, J. M. Luther, Q. Song, B. K. Hughes, C. L. Perkins, A. J. Nozik, *J. Am. Chem. Soc.* **2008**, *130*, 5974.

[28] a) M. Cai, Y. Wu, H. Chen, X. Yang, Y. Qiang, L. Han, *Adv. Sci.* **2017**, *4*, 1600269; b) A. R. Kirmani, *MRS Bull.* **2019**, *44*, 524.

[29] a) K. S. Jeong, J. Tang, H. Liu, J. Kim, A. W. Schaefer, K. Kemp, L. Levina, X. Wang, S. Hoogland, R. Debnath, L. Brzozowski, E. H. Sargent, J. B. Asbury, *ACS Nano* **2012**, *6*, 89; b) E. M. Sanehira, A. R. Marshall, J. A. Christians, S. P. Harvey, J. M. Luther, *Sci. Adv.* **2017**, *3*, eaao4204.

[30] J. M. Luther, M. Law, M. C. Beard, Q. Song, M. O. Reese, R. J. Ellingson, A. J. Nozik, *Nano Lett.* **2008**, *8*, 3488.

[31] a) P. R. Brown, R. R. Lunt, N. Zhao, T. P. Osedach, D. D. Wanger, L.-Y. Chang, M. G. Bawendi, V. Bulović, *Nano Lett.* **2011**, *11*, 2955; b) D. Park, H. Aqoma, I. Ryu, S. Yim, S.-Y. Jang, *IEEE J. Select. Topics Quantum Electron.* **2016**, *22*, 94.

[32] a) A. Stavrinadis, J. M. Smith, C. A. Cattley, A. G. Cook, P. S. Grant, A. A. R. Watt, *Nanotechnology* **2010**, *21*, 185202; b) Z. Ning, D. Zhitomirsky, V. Adinolfi, B. Sutherland, J. Xu, O. Voznyy, P. Maraghechi, X. Lan, S. Hoogland, Y. Ren, E. H. Sargent, *Adv. Mater.* **2013**, *25*, 1719; c) M.-J. Choi, F. P. García de Arquer, A. H. Proppe, A. Seifitokaldani, J. Choi, J. Kim, S.-W. Baek, M. Liu, B. Sun, M. Biondi, B. Scheffel, G. Walters, D.-H. Nam, J. W. Jo, O. Ouellette, O. Voznyy, S. Hoogland, S. O. Kelley, Y. S. Jung, E. H. Sargent, *Nat. Commun.* **2020**, *11*, 103.

[33] a) I. J. Kramer, L. Levina, R. Debnath, D. Zhitomirsky, E. H. Sargent, *Nano Lett.* **2011**, *11*, 3701; b) J. Y. Kim, V. Adinolfi, B. R. Sutherland, O. Voznyy, S. J. Kwon, T. W. Kim, J. Kim, H. Ihee, K. Kemp, M. Adachi, M. Yuan, I. Kramer, D. Zhitomirsky, S. Hoogland, E. H. Sargent, *Nat. Commun.* **2015**, *6*, 7772; c) J. Yuan, C. Bi, J. Xi, R. Guo, J. Tian, *J. Phys. Chem. Lett.* **2021**, *12*, 1018.

[34] J. J. Choi, W. N. Wenger, R. S. Hoffman, Y.-F. Lim, J. Luria, J. Jasieniak, J. A. Marohn, T. Hanrath, *Adv. Mater.* **2011**, *23*, 3144.

[35] M. Hao, Y. Bai, S. Zeiske, L. Ren, J. Liu, Y. Yuan, N. Zarrabi, N. Cheng, M. Ghasemi, P. Chen, M. Lyu, D. He, J.-H. Yun, Y. Du, Y. Wang, S. Ding, A. Armin, P. Meredith, G. Liu, H.-M. Cheng, L. Wang, *Nat. Energy* **2020**, *5*, 79.

[36] a) U. G. Lee, W.-B. Kim, D. H. Han, H. S. Chung, *Symmetry* **2019**, *11*, 1183; b) A. Mishra, N. Bhatt, A. K. Bajpai, in *Nanomaterials-Based Coatings*, Vol. 5, (Eds: P. N. Tri, S. Rtimi, C. M. O. Plamondon), Elsevier, Amsterdam, The Netherlands 2019, Ch. 12; c) G. A. Luurtsema, *Spin Coating for Rectangular Substrates*, University of California, July, **1997**.

[37] Z. Ning, O. Voznyy, J. Pan, S. Hoogland, V. Adinolfi, J. Xu, M. Li, A. R. Kirmani, J.-P. Sun, J. Minor, K. W. Kemp, H. Dong, L. Rollny, A. Labelle, G. Carey, B. Sutherland, I. Hill, A. Amassian, H. Liu, J. Tang, O. M. Bakr, E. H. Sargent, *Nat. Mater.* **2014**, *13*, 822.

[38] G.-H. Kim, F. P. García de Arquer, Y. J. Yoon, X. Lan, M. Liu, O. Voznyy, L. K. Jagadamma, A. S. Abbas, Z. Yang, F. Fan, A. H. Ip, P. Kanjanaboos, S. Hoogland, J. Y. Kim, E. H. Sargent, *Nano Lett.* **2015**, *15*, 7691.

[39] B. Sun, A. Johnston, C. Xu, M. Wei, Z. Huang, Z. Jiang, H. Zhou, Y. Gao, Y. Dong, O. Ouellette, X. Zheng, J. Liu, M.-J. Choi, Y. Gao, S.-W. Baek, F. Laquai, O. M. Bakr, D. Ban, O. Voznyy, F. P. García de Arquer, E. H. Sargent, *Joule* **2020**, *4*, 1542.

[40] a) J. Tang, K. W. Kemp, S. Hoogland, K. S. Jeong, H. Liu, L. Levina, M. Furukawa, X. Wang, R. Debnath, D. Cha, K. W. Chou, A. Fischer, A. Amassian, J. B. Asbury, E. H. Sargent, *Nat. Mater.* **2011**, *10*, 765; b) H. Zhang, B. Hu, L. Sun, R. Hovden, F. W. Wise, D. A. Muller, R. D. Robinson, *Nano Lett.* **2011**, *11*, 5356; c) A. H. Ip, S. M. Thon, S. Hoogland, O. Voznyy, D. Zhitomirsky, R. Debnath, L. Levina, L. R. Rollny, G. H. Carey, A. Fischer, K. W. Kemp, I. J. Kramer, Z. Ning, A. J. Labelle, K. W. Chou, A. Amassian, E. H. Sargent, *Nat. Nanotechnol.* **2012**, *7*, 577; d) D. N. Dirin, S. Dreyfuss, M. I. Bodnarchuk, G. Nedelcu, P. Papagiorgis, G. Itskos, M. V. Kovalenko, *J. Am. Chem. Soc.* **2014**, *136*, 6550; e) R. W. Crisp, D. M. Kroupa, A. R. Marshall, E. M. Miller, J. Zhang, M. C. Beard, J. M. Luther, *Sci. Rep.* **2015**, *5*, 9945; f) D. Jia, J. Chen, M. Yu, J. Liu, E. M. J. Johansson, A. Hagfeldt, X. Zhang, *Small* **2020**, *16*, 2001772; g) J. Khan, X. Zhang, J. Yuan, Y. Wang, G. Shi, R. Patterson, J. Shi, X. Ling, L. Hu, T. Wu, S. Dai, W. Ma, *ACS Energy Lett.* **2020**, *5*, 3322; h) J. Kim, S. Cho, F. Dinic, J. Choi, C. Choi, S. M. Jeong, J.-S. Lee, O. Voznyy, M. J. Ko, Y. Kim, *Nano Energy* **2020**, *75*, 104985; i) Y. Wang, J. Yuan, X. Zhang, X. Ling, B. W. Larson, Q. Zhao, Y. Yang, Y. Shi, J. M. Luther, W. Ma, *Adv. Mater.* **2020**, *32*, 2000449.

[41] a) P. H. Rekemeyer, S. Chang, C.-H. M. Chuang, G. W. Hwang, M. G. Bawendi, S. Gradečak, *Adv. Energy Mater.* **2016**, *6*, 1600848; b) N. Zhang, D. C. J. Neo, Y. Tazawa, X. Li, H. E. Assender, R. G. Compton, A. A. R. Watt, *ACS Appl. Mater. Inter.* **2016**, *8*, 21417; c) J. Choi,

Y. Kim, J. W. Jo, J. Kim, B. Sun, G. Walters, F. P. García de Arquer, R. Quintero-Bermudez, Y. Li, C. S. Tan, L. N. Quan, A. P. T. Kam, S. Hoogland, Z. Lu, O. Voznyy, E. H. Sargent, *Adv. Mater.* **2017**, *29*, 1702350.

[42] S. A. McDonald, G. Konstantatos, S. Zhang, P. W. Cyr, E. J. D. Klem, L. Levina, E. H. Sargent, *Nat. Mater.* **2005**, *4*, 138.

[43] a) R. Vogel, K. Pohl, H. Weller, *Chem. Phys. Lett.* **1990**, *174*, 241; b) I. Robel, V. Subramanian, M. Kuno, P. V. Kamat, *J. Am. Chem. Soc.* **2006**, *128*, 2385; c) J. B. Sambur, B. A. Parkinson, *J. Am. Chem. Soc.* **2010**, *132*, 2130; d) S. Giménez, I. Mora-Seró, L. Macor, N. Guijarro, T. Lana-Villarreal, R. Gómez, L. J. Diguna, Q. Shen, T. Toyoda, J. Bisquert, *Nanotechnology* **2009**, *20*, 295204; e) G. Wang, X. Yang, F. Qian, J. Z. Zhang, Y. Li, *Nano Lett.* **2010**, *10*, 1088.

[44] a) R. Debnath, M. T. Greiner, I. J. Kramer, A. Fischer, J. Tang, D. A. R. Barkhouse, X. Wang, L. Levina, Z.-H. Lu, E. H. Sargent, *Appl. Phys. Lett.* **2010**, *97*, 23109; b) J. M. Luther, J. Gao, M. T. Lloyd, O. E. Semonin, M. C. Beard, A. J. Nozik, *Adv. Mater.* **2010**, *22*, 3704; c) B.-R. Hyun, Y.-W. Zhong, A. C. Bartnik, L. Sun, H. D. Abruña, F. W. Wise, J. D. Goodreau, J. R. Matthews, T. M. Leslie, N. F. Borrelli, *ACS Nano* **2008**, *2*, 2206.

[45] C.-H. M. Chuang, P. R. Brown, V. Bulović, M. G. Bawendi, *Nat. Mater.* **2014**, *13*, 796.

[46] a) X. Lan, O. Voznyy, A. Kiani, F. P. García de Arquer, A. S. Abbas, G.-H. Kim, M. Liu, Z. Yang, G. Walters, J. Xu, M. Yuan, Z. Ning, F. Fan, P. Kanjanaboos, I. Kramer, D. Zhitomirsky, P. Lee, A. Perelgut, S. Hoogland, E. H. Sargent, *Adv. Mater.* **2016**, *28*, 299; b) Z. Yang, A. Janmohamed, X. Lan, F. P. García de Arquer, O. Voznyy, E. Yassitepe, G.-H. Kim, Z. Ning, X. Gong, R. Comin, E. H. Sargent, *Nano Lett.* **2015**, *15*, 7539; c) X. Lan, O. Voznyy, F. P. García de Arquer, M. Liu, J. Xu, A. H. Proppe, G. Walters, F. Fan, H. Tan, M. Liu, Z. Yang, S. Hoogland, E. H. Sargent, *Nano Lett.* **2016**, *16*, 4630.

[47] T. Zhao, E. D. Goodwin, J. Guo, H. Wang, B. T. Diroll, C. B. Murray, C. R. Kagan, *ACS Nano* **2016**, *10*, 9267.

[48] M. Yuan, O. Voznyy, D. Zhitomirsky, P. Kanjanaboos, E. H. Sargent, *Adv. Mater.* **2015**, *27*, 917.

[49] M. Liu, F. P. G. de Arquer, Y. Li, X. Lan, G.-H. Kim, O. Voznyy, L. K. Jagadamma, A. S. Abbas, S. Hoogland, Z. Lu, J. Y. Kim, A. Amassian, E. H. Sargent, *Adv. Mater.* **2016**, *28*, 4142.

[50] a) Y. Zhao, J. S. Marshall, *Physics of Fluids* **2008**, *20*, 43302; b) M. Pichumani, P. Bagheri, K. M. Poduska, W. González-Viñas, A. Yethiraj, *Soft Matter* **2013**, *9*, 3220; c) D. T. W. Toolan, N. Pullan, M. J. Harvey, P. D. Topham, J. R. Howse, *Adv. Mater.* **2013**, *25*, 7033.

[51] a) H. Aqoma, S.-Y. Jang, *Energy Environ. Sci.* **2018**, *11*, 1603; b) A. R. Kirmani, A. D. Sheikh, M. R. Niazi, M. A. Haque, M. Liu, F. P. G. de Arquer, J. Xu, B. Sun, O. Voznyy, N. Gasparini, D. Baran, T. Wu, E. H. Sargent, A. Amassian, *Adv. Mater.* **2018**, *30*, 1801661; c) M.-J. Choi, Y. Kim, H. Lim, E. Alarousu, A. Adhikari, B. S. Shaheen, Y. H. Kim, O. F. Mohammed, E. H. Sargent, J. Y. Kim, Y. S. Jung, *Adv. Mater.* **2019**, *31*, 1805886.

[52] a) A. Kaliyaraj Selva Kumar, Y. Zhang, D. Li, R. G. Compton, *Electrochem. Commun.* **2020**, *121*, 106867; b) G. Tseberlidis, V. Trifiletti, A. Le Donne, L. Frioni, M. Acciarri, S. Binetti, *Sol. Energy* **2020**, *208*, 532.

[53] M. Eslamian, F. Zabihi, *Nanoscale Res. Lett.* **2015**, *10*, 462.

[54] a) Y. Wang, W. Zhou, *J. Nanosci. Nanotechnol.* **2010**, *10*, 1563; b) X. Tang, X. Yan, *J. Sol-Gel Sci. Technol.* **2017**, *81*, 378; c) E. L Scriven, *MRS Online Proc. Libr.* **1988**, *121*, 717.

[55] J. J. Khanam, S. Y. Foo, Z. Yu, T. Liu, P. Mao, *Nanomaterials* **2019**, *9*, 1205.

[56] J. Park, K. Shin, C. Lee, *Int. J. Precis. Eng. Manuf.* **2016**, *17*, 537.

[57] J. M. Luther, M. Law, Q. Song, C. L. Perkins, M. C. Beard, A. J. Nozik, *ACS Nano* **2008**, *2*, 271.

[58] a) J. An, X. Yang, W. Wang, J. Li, H. Wang, Z. Yu, C. Gong, X. Wang, L. Sun, *Sol. Energy* **2017**, *158*, 28; b) K. P. Bhandari, P. J. Roland, H. Mahabaduge, N. O. Haugen, C. R. Grice, S. Jeong, T. Dykstra, J. Gao, R. J. Ellingson, *Sol. Energy Mater. Sol. Cells* **2013**, *117*, 476; c) W. Xu, F. Tan, Q. Liu, X. Liu, Q. Jiang, L. Wei, W. Zhang, Z. Wang, S. Qu, Z. Wang, *Sol. Energy Mater. Sol. Cells* **2017**, *159*, 503.

[59] Z. Zhang, Z. Chen, L. Yuan, W. Chen, J. Yang, B. Wang, X. Wen, J. Zhang, L. Hu, J. A. Stride, G. J. Conibeer, R. J. Patterson, S. Huang, *Adv. Mater.* **2017**, *29*, 1703214.

[60] Z. Zhang, Z. Chen, J. Zhang, W. Chen, J. Yang, X. Wen, B. Wang, N. Kobamoto, L. Yuan, J. A. Stride, G. J. Conibeer, R. J. Patterson, S. Huang, *Adv. Energy Mater.* **2017**, *7*, 1601773.

[61] D. Grosso, *J. Mater. Chem.* **2011**, *21*, 17033.

[62] S. Maenosono, T. Okubo, Y. Yamaguchi, *J. Nanopart. Res.* **2003**, *5*, 5.

[63] G. H. Carey, A. L. Abdelhady, Z. Ning, S. M. Thon, O. M. Bakr, E. H. Sargent, *Chem. Rev.* **2015**, *115*, 12732.

[64] I. J. Kramer, J. C. Minor, G. Moreno-Bautista, L. Rollny, P. Kanjanaboos, D. Kopilovic, S. M. Thon, G. H. Carey, K. W. Chou, D. Zhitomirsky, A. Amassian, E. H. Sargent, *Adv. Mater.* **2015**, *27*, 116.

[65] J. E. Bishop, T. J. Routledge, D. G. Lidzey, *J. Phys. Chem. Lett.* **2018**, *9*, 1977.

[66] V. A. Akhavan, B. W. Goodfellow, M. G. Panthani, D. K. Reid, D. J. Hellebusch, T. Adachi, B. A. Korgel, *Energy Environ. Sci.* **2010**, *3*, 1600.

[67] E. E. Foos, W. Yoon, M. P. Lumb, J. G. Tischler, T. K. Townsend, *ACS Appl. Mater. Inter.* **2013**, *5*, 8828.

[68] I. J. Kramer, G. Moreno-Bautista, J. C. Minor, D. Kopilovic, E. H. Sargent, *Appl. Phys. Lett.* **2014**, *105*, 163902.

[69] H. Choi, J.-G. Lee, X. D. Mai, M. C. Beard, S. S. Yoon, S. Jeong, *Sci. Rep.* **2017**, *7*, 622.

[70] J. Yuan, C. Bi, S. Wang, R. Guo, T. Shen, L. Zhang, J. Tian, *Adv. Funct. Mater.* **2019**, *29*, 1906615.

[71] a) Y. Zhao, F. Ma, F. Gao, Z. Yin, X. Zhang, J. You, *Photon. Res.* **2020**, *8*, A1; b) R. Sliz, M. Lejay, J. Z. Fan, M.-J. Choi, S. Kinge, S. Hoogland, T. Fabritius, F. P. García de Arquer, E. H. Sargent, *ACS Nano* **2019**, *13*, 11988; c) S. Shi, W. Bai, T. Xuan, T. Zhou, G. Dong, R.-J. Xie, *Small Methods* **2021**, *5*, 2000889.

[72] S. K. Karunakaran, G. M. Arumugam, W. Yang, S. Ge, S. N. Khan, X. Lin, G. Yang, *J. Mater. Chem. A* **2019**, *7*, 13873.

[73] F. Mathies, E. J. W. List-Kratochvil, E. L. Unger, *Energy Technol.* **2020**, *8*, 1900991.

[74] a) P. Yang, L. Zhang, D. J. Kang, R. Strahl, T. Kraus, *Adv. Optical Mater.* **2020**, *8*, 1901429; b) Y. Liu, F. Li, Z. Xu, C. Zheng, T. Guo, X. Xie, L. Qian, D. Fu, X. Yan, *ACS Appl. Mater. Inter.* **2017**, *9*, 25506; c) C. Xiang, L. Wu, Z. Lu, M. Li, Y. Wen, Y. Yang, W. Liu, T. Zhang, W. Cao, S.-W. Tsang, B. Shan, X. Yan, L. Qian, *Nat. Commun.* **2020**, *11*, 1646.

[75] G. H. McKinley, M. Renardy, *Phys. Fluids* **2011**, *23*, 127101.

[76] G. Konvalina, A. Leshansky, H. Haick, *Adv. Funct. Mater.* **2015**, *25*, 2411.

[77] F. Doumenc, J.-B. Salmon, B. Guerrier, *Langmuir* **2016**, *32*, 13657.

[78] N.-G. Park, K. Zhu, *Nat. Rev. Mater.* **2020**, *5*, 333.

[79] M. Joshi, B. S. Butola, in *Advances in the Dyeing and Finishing of Technical Textiles*, (Ed: M. L. Gulrajani), Woodhead Publishing, Cambridge, England **2013**, Ch. 14.

[80] a) W.-K. Koh, S. R. Saudari, A. T. Fafarman, C. R. Kagan, C. B. Murray, *Nano Lett.* **2011**, *11*, 4764; b) H. Zhang, J. Jang, W. Liu, D. V. Talapin, *ACS Nano* **2014**, *8*, 7359; c) O. Jiménez Farías, C. Lombard Latune, S. P. Walborn, L. Davidovich, P. H. Souto Ribeiro, *Science* **2009**, *324*, 1414.

[81] M. Mennig, M. A. Aegerter, *Sol-Gel Technologies for Glass Producers and Users*, Springer, Boston, MA **2004**.

[82] X. Ding, J. Liu, T. A. L. Harris, *AIChE J.* **2016**, *62*, 2508.

[83] a) Y. Galagan, F. Di Giacomo, H. Gorter, G. Kirchner, I. de Vries, R. Andriessen, P. Groen, *Adv. Energy Mater.* **2018**, *8*, 1801935; b) T. Bu, J. Li, F. Zheng, W. Chen, X. Wen, Z. Ku, Y. Peng, J. Zhong, Y.-B. Cheng, F. Huang, *Nat. Commun.* **2018**, *9*, 4609; c) Y. Zhao, G. Wang, Y. Wang, T. Xiao, M. A. Adil, G. Lu, J. Zhang, Z. Wei, *Sol. RRL* **2019**, *3*, 1800333.

[84] M. Fievez, P. J. Singh Rana, T. M. Koh, M. Manceau, J. H. Lew, N. F. Jamaludin, B. Ghosh, A. Bruno, S. Cros, S. Berson, S. G. Mhaisalkar, W. L. Leong, *Sol. Energy Mater. Sol. Cells* **2021**, *230*, 111189.

[85] a) Ossila, Solution-Processing Techniques: A Comparison, https://www.ossila.com/pages/solution-processing-techniques-comparison, accessed: October, **2021**; b) M. D. Tyona, *Adv. Mater. Res.* **2013**, *2*, 195.

[86] a) A. R. Kirmani, *MRS Bull.* **2019**, *44*, 524; b) nTact, Slot Die Coating Technology, https://ntact.com/applications/slot-die-coating, accessed: November, **2013**.

[87] A. Dey, J. Ye, A. De, E. Debroye, S. K. Ha, E. Bladt, A. S. Kshirsagar, Z. Wang, J. Yin, Y. Wang, L. N. Quan, F. Yan, M. Gao, X. Li, J. Shamsi, T. Debnath, M. Cao, M. A. Scheel, S. Kumar, J. A. Steele, M. Gerhard, L. Chouhan, K. Xu, X.-G. Wu, Y. Li, Y. Zhang, A. Dutta, C. Han, I. Vincon, A. L. Rogach, A. Nag, A. Samanta, B. A. Korgel, C.-J. Shih, D. R. Gamelin, D. H. Son, H. Zeng, H. Zhong, H. Sun, H. V. Demir, I. G. Scheblykin, I. Mora-Seró, J. K. Stolarczyk, J. Z. Zhang, J. Feldmann, J. Hofkens, J. M. Luther, J. Pérez-Prieto, L. Li, L. Manna, M. I. Bodnarchuk, M. V. Kovalenko, M. B. J. Roeffaers, N. Pradhan, O. F. Mohammed, O. M. Bakr, P. Yang, P. Müller-Buschbaum, P. V. Kamat, Q. Bao, Q. Zhang, R. Krahne, R. E. Galian, S. D. Stranks, S. Bals, V. Biju, W. A. Tisdale, Y. Yan, R. L. Z. Hoye, L. Polavarapu, *ACS Nano* **2021**, *15*, 10775.

[88] L. C. Schmidt, A. Pertegás, S. González-Carrero, O. Malinkiewicz, S. Agouram, G. Mínguez Espallargas, H. J. Bolink, R. E. Galian, J. Pérez-Prieto, *J. Am. Chem. Soc.* **2014**, *136*, 850.

[89] Q. Zhao, A. Hazarika, L. T. Schelhas, J. Liu, E. A. Gaulding, G. Li, M. Zhang, M. F. Toney, P. C. Sercel, J. M. Luther, *ACS Energy Lett.* **2020**, *5*, 238.

[90] A. Inbal, J. P. Ampuero, R. W. Clayton, *Science* **2016**, *354*, 88.

[91] L. M. Wheeler, E. M. Sanehira, A. R. Marshall, P. Schulz, M. Suri, N. C. Anderson, J. A. Christians, D. Nordlund, D. Sokaras, T. Kroll, S. P. Harvey, J. J. Berry, L. Y. Lin, J. M. Luther, *J. Am. Chem. Soc.* **2018**, *140*, 10504.

[92] J. Kim, B. Koo, W. H. Kim, J. Choi, C. Choi, S. J. Lim, J.-S. Lee, D.-H. Kim, M. J. Ko, Y. Kim, *Nano Energy* **2019**, *66*, 104130.

[93] R. Han, Q. Zhao, J. Su, X. Zhou, X. Ye, X. Liang, J. Li, H. Cai, J. Ni, J. Zhang, *J. Phys. Chem. C* **2021**, *125*, 8469.

[94] a) Y. Bai, M. Hao, S. Ding, P. Chen, L. Wang, *Adv. Mater.* **2021**, 2105958; b) J. Chen, D. Jia, E. M. J. Johansson, A. Hagfeldt, X. Zhang, *Energy Environ. Sci.* **2021**, *14*, 224.

[95] Q. Wang, Z. Jin, D. Chen, D. Bai, H. Bian, J. Sun, G. Zhu, G. Wang, S. F. Liu, *Adv. Energy Mater.* **2018**, *8*, 1800007.

[96] X. Ling, S. Zhou, J. Yuan, J. Shi, Y. Qian, B. W. Larson, Q. Zhao, C. Qin, F. Li, G. Shi, C. Stewart, J. Hu, X. Zhang, J. M. Luther, S. Duhm, W. Ma, *Adv. Energy Mater.* **2019**, *9*, 1900721.

[97] a) X. Zhu, M. Du, J. Feng, H. Wang, Z. Xu, L. Wang, S. Zuo, C. Wang, Z. Wang, C. Zhang, X. Ren, S. Priya, D. Yang, S. F. Liu, *Angew. Chem., Int. Ed.* **2021**, *60*, 4238; b) X. Mao, P. Brown, C. Červinka, G. Hazell, H. Li, Y. Ren, Di Chen, R. Atkin, J. Eastoe, I. Grillo, A. A. H. Padua, M. F. Costa Gomes, T. A. Hatton, *Nat. Mater.* **2019**, *18*, 1350.

[98] S. Wang, A. A. Yousefi Amin, L. Wu, M. Cao, Q. Zhang, T. Ameri, *Small Struct.* **2021**, *2*, 2000124.

[99] S. Cho, J. Kim, S. M. Jeong, M. J. Ko, J.-S. Lee, Y. Kim, *Chem. Mater.* **2020**, *32*, 8808.

[100] J. Xue, J.-W. Lee, Z. Dai, R. Wang, S. Nuryyeva, M. E. Liao, S.-Y. Chang, L. Meng, D. Meng, P. Sun, O. Lin, M. S. Goorsky, Y. Yang, *Joule* **2018**, *2*, 1866.

[101] J. Kim, S. Cho, F. Dinic, J. Choi, C. Choi, S. M. Jeong, J.-S. Lee, O. Voznyy, M. J. Ko, Y. Kim, *Nano Energy* **2020**, *75*, 104985.

[102] L.-J. Chen, C.-R. Lee, Y.-J. Chuang, Z.-H. Wu, C. Chen, *J. Phys. Chem. Lett.* **2016**, *7*, 5028.

[103] F. Liu, C. Ding, Y. Zhang, T. S. Ripolles, T. Kamisaka, T. Toyoda, S. Hayase, T. Minemoto, K. Yoshino, S. Dai, M. Yanagida, H. Noguchi, Q. Shen, *J. Am. Chem. Soc.* **2017**, *139*, 16708.

[104] Y. Wang, J. Tu, T. Li, C. Tao, X. Deng, Z. Li, *J. Mater. Chem. A* **2019**, *7*, 7683.

[105] S. Christodoulou, F. Di Stasio, S. Pradhan, A. Stavrinadis, G. Konstantatos, *J. Phys. Chem. C* **2018**, *122*, 7621.

[106] C. Liu, Y. Yang, X. Liu, Y. Ding, Z. Arain, X. Li, Y. Li, Z. Zhou, S. Dai, M. K. Nazeeruddin, *J. Mater. Chem. A* **2020**, *8*, 10226.

[107] K. Chen, Q. Zhong, W. Chen, B. Sang, Y. Wang, T. Yang, Y. Liu, Y. Zhang, H. Zhang, *Adv. Funct. Mater.* **2019**, *29*, 1900991.

[108] Y. Wang, J. Yuan, X. Zhang, X. Ling, B. W. Larson, Q. Zhao, Y. Yang, Y. Shi, J. M. Luther, W. Ma, *Adv. Mater.* **2020**, *32*, 2000449.

[109] N. Guijarro, L. Yao, F. Le Formal, R. A. Wells, Y. Liu, B. P. Darwich, L. Navratilova, H.-H. Cho, J.-H. Yum, K. Sivula, *Angew. Chem., Int. Ed.* **2019**, *58*, 12696.

[110] J. Khan, X. Zhang, J. Yuan, Y. Wang, G. Shi, R. Patterson, J. Shi, X. Ling, L. Hu, T. Wu, S. Dai, W. Ma, *ACS Energy Lett.* **2020**, *5*, 3322.

[111] X. Ling, J. Yuan, X. Zhang, Y. Qian, S. M. Zakeeruddin, B. W. Larson, Q. Zhao, J. Shi, J. Yang, K. Ji, Y. Zhang, Y. Wang, C. Zhang, S. Duhm, J. M. Luther, M. Grätzel, W. Ma, *Adv. Mater.* **2020**, *32*, 2001906.

[112] D. Jia, J. Chen, M. Yu, J. Liu, E. M. J. Johansson, A. Hagfeldt, X. Zhang, *Small* **2020**, *16*, 2001772.

[113] D. Jia, J. Chen, X. Mei, W. Fan, S. Luo, M. Yu, J. Liu, X. Zhang, *Energy Environ. Sci.* **2021**, *14*, 4599.

[114] J. Shi, F. Li, Y. Jin, C. Liu, B. Cohen-Kleinstein, S. Yuan, Y. Li, Z.-K. Wang, J. Yuan, W. Ma, *Angew. Chem., Int. Ed.* **2020**, *59*, 22230.

[115] Y. Dong, Y.-K. Wang, F. Yuan, A. Johnston, Y. Liu, D. Ma, M.-J. Choi, B. Chen, M. Chekini, S.-W. Baek, L. K. Sagar, J. Fan, Y. Hou, M. Wu, S. Lee, B. Sun, S. Hoogland, R. Quintero-Bermudez, H. Ebe, P. Todorovic, F. Dinic, P. Li, H. T. Kung, M. I. Saidaminov, E. Kumacheva, E. Spiecker, L.-S. Liao, O. Voznyy, Z.-H. Lu, E. H. Sargent, *Nat. Nanotechnol.* **2020**, *15*, 668.

[116] G. Li, J. Huang, Y. Li, J. Tang, Y. Jiang, *Nano Res.* **2019**, *12*, 109.

[117] S. Baek, Y. Kim, S.-W. Kim, *J. Ind. Eng. Chem.* **2020**, *83*, 279.

[118] M.-J. Choi, F. P. García de Arquer, A. H. Proppe, A. Seifitokaldani, J. Choi, J. Kim, S.-W. Baek, M. Liu, B. Sun, M. Biondi, B. Scheffel, G. Walters, D.-H. Nam, J. W. Jo, O. Ouellette,

O. Voznyy, S. Hoogland, S. O. Kelley, Y. S. Jung, E. H. Sargent, *Nat. Commun.* **2020**, *11*, 103.

[119] Q. Xie, D. Wu, X. Wang, Y. Li, F. Fang, Z. Wang, Y. Ma, M. Su, S. Peng, H. Liu, K. Wang, X. W. Sun, *J. Mater. Chem. C* **2019**, *7*, 11251.

[120] Y.-H. Suh, T. Kim, J. W. Choi, C.-L. Lee, J. Park, *ACS Appl. Nano Mater.* **2018**, *1*, 488.

[121] J. H. Park, A.-Y. Lee, J. C. Yu, Y. S. Nam, Y. Choi, J. Park, M. H. Song, *ACS Appl. Mater. Inter.* **2019**, *11*, 8428.

[122] C. Bi, S. V. Kershaw, A. L. Rogach, J. Tian, *Adv. Funct. Mater.* **2019**, *29*, 1902446.

[123] J. Pan, L. N. Quan, Y. Zhao, W. Peng, B. Murali, S. P. Sarmah, M. Yuan, L. Sinatra, N. M. Alyami, J. Liu, E. Yassitepe, Z. Yang, O. Voznyy, R. Comin, M. N. Hedhili, O. F. Mohammed, Z. H. Lu, D. H. Kim, E. H. Sargent, O. M. Bakr, *Adv. Mater.* **2016**, *28*, 8718.

[124] C. Bi, Z. Yao, X. Sun, X. Wei, J. Wang, J. Tian, *Adv. Mater.* **2021**, *33*, 2006722.

[125] L. Hu, Q. Zhao, S. Huang, J. Zheng, X. Guan, R. Patterson, J. Kim, L. Shi, C.-H. Lin, Q. Lei, D. Chu, W. Tao, S. Cheong, R. D. Tilley, A. W. Y. Ho-Baillie, J. M. Luther, J. Yuan, T. Wu, *Nat. Commun.* **2021**, *12*, 466.

[126] K. Ji, J. Yuan, F. Li, Y. Shi, X. Ling, X. Zhang, Y. Zhang, H. Lu, J. Yuan, W. Ma, *J. Mater. Chem. A* **2020**, *8*, 8104.

[127] a) K. Chen, Q. Zhong, W. Chen, B. Sang, Y. Wang, T. Yang, Y. Liu, Y. Zhang, H. Zhang, *Adv. Funct. Mater.* **2019**, *29*, 1900991; b) F. Liu, C. Ding, Y. Zhang, T. Kamisaka, Q. Zhao, J. M. Luther, T. Toyoda, S. Hayase, T. Minemoto, K. Yoshino, B. Zhang, S. Dai, J. Jiang, S. Tao, Q. Shen, *Chem. Mater.* **2019**, *31*, 798; c) J. Shi, F. Li, J. Yuan, X. Ling, S. Zhou, Y. Qian, W. Ma, *J. Mater. Chem. A* **2019**, *7*, 20936; d) C. Bi, X. Sun, X. Huang, S. Wang, J. Yuan, J. X. Wang, T. Pullerits, J. Tian, *Chem. Mater.* **2020**, *32*, 6105; e) K. Chen, W. Jin, Y. Zhang, T. Yang, P. Reiss, Q. Zhong, U. Bach, Q. Li, Y. Wang, H. Zhang, Q. Bao, Y. Liu, *J. Am. Chem. Soc.* **2020**, *142*, 3775; f) Z. Zang, D. Yan, in *Perovskite Quantum Dots*, Vol. 303 (Eds.: Y. Zhou, Y. Wang), Springer Singapore. Singapore **2020**, Ch. 3.

[128] Z. Li, M. Yang, J.-S. Park, S.-H. Wei, J. J. Berry, K. Zhu, *Chem. Mater.* **2016**, *28*, 284.

[129] M. Shrivastava, M. I. Bodnarchuk, A. Hazarika, J. M. Luther, M. C. Beard, M. V. Kovalenko, K. V. Adarsh, *Adv. Opt. Mater.* **2020**, *8*, 2001016.

[130] J. Xue, J.-W. Lee, Z. Dai, R. Wang, S. Nuryyeva, M. E. Liao, S.-Y. Chang, L. Meng, D. Meng, P. Sun, O. Lin, M. S. Goorsky, Y. Yang, *Joule* **2018**, *2*, 1866.

[131] J. Xue, R. Wang, L. Chen, S. Nuryyeva, T.-H. Han, T. Huang, S. Tan, J. Zhu, M. Wang, Z.-K. Wang, C. Zhang, J.-W. Lee, Y. Yang, *Adv. Mater.* **2019**, *31*, 1900111.

[132] V. L. Pool, B. Dou, D. G. van Campen, T. R. Klein-Stockert, F. S. Barnes, S. E. Shaheen, M. I. Ahmad, M. F. A. M. van Hest, M. F. Toney, *Nat. Commun.* **2017**, *8*, 14075.

[133] F. Li, S. Zhou, J. Yuan, C. Qin, Y. Yang, J. Shi, X. Ling, Y. Li, W. Ma, *ACS Energy Lett.* **2019**, *4*, 2571.

[134] a) G.-X. Li, Q. Li, R. Cheng, S. Chen, *Curr. Opin. Chem. Eng.* **2020**, *29*, 34; b) K. Abdel-Latif, F. Bateni, S. Crouse, M. Abolhasani, *Matter* **2020**, *3*, 1053; c) S. Kubendhiran, Z. Bao, K. Dave, R.-S. Liu, *ACS Appl. Nano Mater.* **2019**, *2*, 1773.

[135] Q. A. Akkerman, M. Gandini, F. Di Stasio, P. Rastogi, F. Palazon, G. Bertoni, J. M. Ball, M. Prato, A. Petrozza, L. Manna, *Nat. Energy* **2017**, *2*, 141.

[136] S. Panigrahi, S. Jana, T. Calmeiro, D. Nunes, R. Martins, E. Fortunato, *ACS Nano* **2017**, *11*, 10214.

[137] S. Christodoulou, F. Di Stasio, S. Pradhan, A. Stavrinadis, G. Konstantatos, *J. Phys. Chem. C* **2018**, *122*, 7621.

[138] D. Ghosh, M. Y. Ali, D. K. Chaudhary, S. Bhattacharyya, *Sol. Energy Mater. Sol. Cells* **2018**, *185*, 28.

[139] Z. Zolfaghari, E. Hassanabadi, D. Pitarch-Tena, S. J. Yoon, Z. Shariatinia, J. van de Lagemaat, J. M. Luther, I. Mora-Seró, *ACS Energy Lett.* **2019**, *4*, 251.

[140] M. M. Tavakoli, M. Nasilowski, J. Zhao, M. G. Bawendi, J. Kong, *Small Methods* **2019**, *3*, 1900449.

[141] T. Yang, Z. Zhang, Y. Ding, N. Yin, X. Liu, *J. Nanopart. Res.* **2019**, *21*,13422.

[142] C. Ding, F. Liu, Y. Zhang, D. Hirotani, X. Rin, S. Hayase, T. Minemoto, T. Masuda, R. Wang, Q. Shen, *Nano Energy* **2020**, *67*, 104267.

[143] Y. Liu, X. Zhao, Z. Yang, Q. Li, W. Wei, B. Hu, W. Chen, *ACS Appl. Energy Mater.* **2020**, *3*, 3521.

[144] S. B. Shivarudraiah, M. Ng, C.-H. A. Li, J. E. Halpert, *ACS Appl. Energy Mater.* **2020**, *3*, 5620.

[145] J. Shi, F. Li, Y. Jin, C. Liu, B. Cohen-Kleinstein, S. Yuan, Y. Li, Z.-K. Wang, J. Yuan, W. Ma, *Angew. Chem., Int. Ed.* **2020**, *59*, 22230.

[146] C. Xiao, Q. Zhao, C.-S. Jiang, Y. Sun, M. M. Al-Jassim, S. U. Nanayakkara, J. M. Luther, *Nano Energy* **2020**, *78*, 105319.

[147] S. Cho, J. Kim, S. M. Jeong, M. J. Ko, J.-S. Lee, Y. Kim, *Chem. Mater.* **2020**, *32*, 8808.

[148] J. Yuan, X. Zhang, J. Sun, R. Patterson, H. Yao, Di Xue, Y. Wang, K. Ji, L. Hu, S. Huang, D. Chu, T. Wu, J. Hou, J. Yuan, *Adv. Funct. Mater.* **2021**, *31*, 2101272.

[149] S. Y. Park, H. C. Shim, *ACS Appl. Mater. Inter.* **2020**, *12*, 57124.

[150] S. Lim, J. Kim, J. Y. Park, J. Min, S. Yun, T. Park, Y. Kim, J. Choi, *ACS Appl. Mater. Inter.* **2021**, *13*, 6119.

[151] L. Zhang, C. Kang, G. Zhang, Z. Pan, Z. Huang, S. Xu, H. Rao, H. Liu, S. Wu, X. Wu, X. Li, Z. Zhu, X. Zhong, A. K.-Y. Jen, *Adv. Funct. Mater.* **2021**, *31*, 2005930.

[152] D. Ghosh, M. Y. Ali, A. Ghosh, A. Mandal, S. Bhattacharyya, *J. Phys. Chem. C* **2021**, *125*, 5485.

[153] Y. Wang, C. Duan, X. Zhang, J. Sun, X. Ling, J. Shi, L. Hu, Z. Zhou, X. Wu, W. Han, X. Liu, C. Cazorla, D. Chu, S. Huang, T. Wu, J. Yuan, W. Ma, *Adv. Funct. Mater.* **2021**, 2108615.

[154] Y. Liu, Q. Li, W. Zhang, Z. Yang, S. Zhao, W. Chen, *ACS Appl. Energy Mater.* **2021**, *4*, 6688.

[155] X. Huang, J. Hu, C. Bi, J. Yuan, Y. Lu, M. Sui, J. Tian, *Chem. Eng. J.* **2021**, *421*, 127822.

[156] A. Babayigit, D. Duy Thanh, A. Ethirajan, J. Manca, M. Muller, H.-G. Boyen, B. Conings, *Sci. Rep.* **2016**, *6*, 18721.

[157] J. Rodríguez-Romero, J. Sanchez-Diaz, C. Echeverría-Arrondo, S. Masi, D. Esparza, E. M. Barea, I. Mora-Seró, *ACS Energy Lett.* **2020**, *5*, 1013.

[158] J. Jean, J. Xiao, R. Nick, N. Moody, M. Nasilowski, M. Bawendi, V. Bulović, *Energy Environ. Sci.* **2018**, *11*, 2295.

[159] M.-G. Ju, M. Chen, Y. Zhou, J. Dai, L. Ma, N. P. Padture, X. C. Zeng, *Joule* **2018**, *2*, 1231.

[160] A. L. Wani, A. Ara, J. A. Usmani, *Interdiscip. Toxicol.* **2015**, *8*, 55.

[161] a) E. Rubin, D. S. Strayer, *Rubin's Pathology: Clinicopathologic Foundations of Medicine*, Wolters Kluwer/Lippincott Williams & Wilkins, Philadelphia, PA, USA **2008**.; b) S. A. Hoda, R. S. Hoda, *J. Am. Med. Assoc.* **2007**, *298*, 2070.

[162] M. Goldberg, S. M. Levin, J. T. Doucette, G. Griffin, *Am. J. Ind. Med.* **1997**, *31*, 310.

[163] a) B. Saparov, F. Hong, J.-P. Sun, H.-S. Duan, W. Meng, S. Cameron, I. G. Hill, Y. Yan, D. B. Mitzi, *Chem. Mater.* **2015**, *27*, 5622; b) A. H. Slavney, T. Hu, A. M. Lindenberg, H. I. Karunadasa, *J. Am. Chem. Soc.* **2016**, *138*, 2138; c) G. Volonakis, A. A. Haghighirad, R. L.

Milot, W. H. Sio, M. R. Filip, B. Wenger, M. B. Johnston, L. M. Herz, H. J. Snaith, F. Giustino, *J. Phys. Chem. Lett.* **2017**, *8*, 772.

[164] Y. Tang, S. Tang, M. Luo, Y. Guo, Y. Zheng, Y. Lou, Y. Zhao, *Chem. Commun.* **2021**, *57*, 7465.

[165] a) F. Giustino, H. J. Snaith, *ACS Energy Lett.* **2016**, *1*, 1233; b) B. Yang, J. Chen, F. Hong, X. Mao, K. Zheng, S. Yang, Y. Li, T. Pullerits, W. Deng, K. Han, *Angew. Chem., Int. Ed.* **2017**, *56*, 12471.

[166] a) J. Sun, J. Yang, J. I. Lee, J. H. Cho, M. S. Kang, *J. Phys. Chem. Lett.* **2018**, *9*, 1573; b) N. Ding, D. Zhou, G. Pan, W. Xu, X. Chen, D. Li, X. Zhang, J. Zhu, Y. Ji, H. Song, *ACS Sustainable Chem. Eng.* **2019**, *7*, 8397; c) Q. Fan, G. V. Biesold-McGee, J. Ma, Q. Xu, S. Pan, J. Peng, Z. Lin, *Angew. Chem., Int. Ed.* **2020**, *59*, 1030.

[167] Q. Liu, J. Yin, B.-B. Zhang, J.-K. Chen, Y. Zhou, L.-M. Zhang, L.-M. Wang, Q. Zhao, J. Hou, J. Shu, B. Song, N. Shirahata, O. M. Bakr, O. F. Mohammed, H.-T. Sun, *J. Am. Chem. Soc.* **2021**, *143*, 5470.

[168] R. Akçan, H. C. Aydogan, M. Ş. Yildirim, B. Taştekin, N. Sağlam, *Turkish J. Med. Sci.* **2020**, *50*, 1180.

[169] T. Moot, D. R. Dikova, A. Hazarika, T. H. Schloemer, S. N. Habisreutinger, N. Leick, S. P. Dunfield, B. A. Rosales, S. P. Harvey, J. R. Pfeilsticker, G. Teeter, L. M. Wheeler, B. W. Larson, J. M. Luther, *Chem. Mater.* **2020**, *32*, 7850.

[170] a) T. Leijtens, G. E. Eperon, N. K. Noel, S. N. Habisreutinger, A. Petrozza, H. J. Snaith, *Adv. Energy Mater.* **2015**, *5*, 1500963; b) Y. Rong, L. Liu, A. Mei, X. Li, H. Han, *Adv. Energy Mater.* **2015**, *5*, 1501066.

[171] A. Loiudice, S. Saris, E. Oveisi, D. T. L. Alexander, R. Buonsanti, *Angew. Chem., Int. Ed.* **2017**, *56*, 10696.

[172] a) Z. Shi, Y. Li, Y. Zhang, Y. Chen, X. Li, Di Wu, T. Xu, C. Shan, G. Du, *Nano Lett.* **2017**, *17*, 313; b) Z. Shi, S. Li, Y. Li, H. Ji, X. Li, Di Wu, T. Xu, Y. Chen, Y. Tian, Y. Zhang, C. Shan, G. Du, *ACS Nano* **2018**, *12*, 1462.

[173] N. L. Chang, A. W. Y. Ho-Baillie, D. Vak, M. Gao, M. A. Green, R. J. Egan, *Sol. Energy Mater. Sol. Cells* **2018**, *174*, 314.

[174] V. Benda, L. Černá, *Heliyon* **2020**, *6*, e05666.

[175] K. Ramanathan, L. Mansfield, C. Deline, T. Silverman, R. Garris, present at NREL PV Module Reliability Workshop, U.S. Golden CO, February, **2015**.

[176] U.S. Energy Information Administration. Levelized Costs of New Generation Resources, https://www.eia.gov/outlooks/aeo/electricity_generation.php, accessed: February, **2021**.

[177] a) C. Wadia, A. P. Alivisatos, D. M. Kammen, *Environ. Sci. Technol.* **2009**, *43*, 2072; b) J. Jean, P. R. Brown, R. L. Jaffe, T. Buonassisi, V. Bulović, *Energy Environ. Sci.* **2015**, *8*, 1200.

[178] T. Wang, X. Li, T. Fang, S. Wang, J. Song, *Chem. Eng. J.* **2021**, *418*, 129361.

[179] a) K. Abdel-Latif, R. W. Epps, F. Bateni, S. Han, K. G. Reyes, M. Abolhasani, *Adv. Intell. Syst.* **2021**, *3*, 2000245; b) L. Wang, L. R. Karadaghi, R. L. Brutchey, N. Malmstadt, *Chem. Commun.* **2020**, *56*, 3745; c) I. Lignos, S. Stavrakis, G. Nedelcu, L. Protesescu, A. J. deMello, M. V. Kovalenko, *Nano Lett.* **2016**, *16*, 1869.

[180] J. M. Ball, S. D. Stranks, M. T. Hörantner, S. Hüttner, W. Zhang, E. J. W. Crossland, I. Ramirez, M. Riede, M. B. Johnston, R. H. Friend, H. J. Snaith, *Energy Environ. Sci.* **2015**, *8*, 602.

[181] X. Zhang, H. Huang, X. Ling, J. Sun, X. Jiang, Y. Wang, Di Xue, L. Huang, L. Chi, J. Yuan, W. Ma, *Adv. Mater.* **2021**, 2105977.

[182] a) A. J. Nozik, M. C. Beard, J. M. Luther, M. Law, R. J. Ellingson, J. C. Johnson, *Chem. Rev.* **2010**, *110*, 6873; b) M. C. Beard, *J. Phys. Chem. Lett.* **2011**, *2*, 1282.

[183] a) M. Li, J. Fu, Q. Xu, T. C. Sum, *Adv. Mater.* **2019**, *31*, 1802486; b) Z. Guo, Y. Wan, M. Yang, J. Snaider, K. Zhu, L. Huang, *Science* **2017**, *356*, 59.

[184] a) T. J. Milstein, K. T. Kluherz, D. M. Kroupa, C. S. Erickson, J. J. de Yoreo, D. R. Gamelin, *Nano Lett.* **2019**, *19*, 1931; b) D. M. Kroupa, J. Y. Roh, T. J. Milstein, S. E. Creutz, D. R. Gamelin, *ACS Energy Lett.* **2018**, *3*, 2390.

[185] K. Kobbekaduwa, E. Liu, Q. Zhao, P. Adhikari, C. Xie, J. Zhang, Y. Shi, H. Zheng, D. Li, H. Sanabria, M. Hu, T. Cai, O. Chen, R. Rao, A. Rao, M. Beard, J. Luther, J. Gao, *Research Square*, 10.21203/rs.3.rs-912920/v1, 1, submitted: September, **2021**

[186] a) X. Zheng, B. Chen, J. Dai, Y. Fang, Y. Bai, Y. Lin, H. Wei, X. C. Zeng, J. Huang, *Nat. Energy* **2017**, *2*, 6503; b) Q. Jiang, Y. Zhao, X. Zhang, X. Yang, Y. Chen, Z. Chu, Q. Ye, X. Li, Z. Yin, J. You, *Nat. Photonics* **2019**, *13*, 460.

[187] B. M. Wieliczka, J. A. Márquez, A. M. Bothwell, Q. Zhao, T. Moot, K. T. VanSant, A. J. Ferguson, T. Unold, D. Kuciauskas, J. M. Luther, *ACS Nano*, DOI: 10.1021/acsnano.1c05642.

Author biographies

Qian Zhao is a postdoctoral researcher in School of Materials Science and Engineering at Nankai University. He completed the doctoral research on "Fundamental properties of perovskite quantum dots toward high efficiency solar cells" under Joseph M. Luther's supervision at National Renewable Energy Laboratory and received his PhD degree in physical chemistry in 2020. His current research interests include synthesis of the perovskite quantum dots, understanding quantum dot properties and developing high-performance perovskite solar cells as well as other photovoltaic applications.

Abhijit Hazarika is a Scientist at the CSIR-Indian Institute of Chemical Technology, Hyderabad, India. He received his PhD in Chemistry from Indian Institute of Science, Bangalore in 2015 followed by Post-Doctoral research experiences at the University of Chicago and the National Renewable Energy Laboratory (NREL) respectively. His research interests focus mainly on design and synthesis of colloidal nanomaterials for optoelectronic applications along with deeper understanding of the photophysical properties and structure-property relationships.

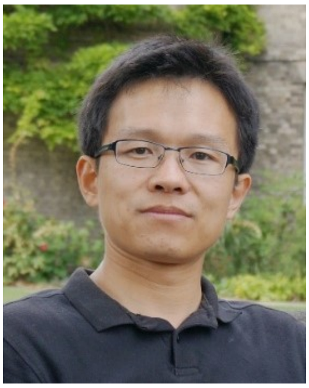

Guo-Ran Li is a full professor at the School of Material Science and Engineering, Nankai University, China. His main current research interest is the study of new energy materials and devices, and in particular for hybrid solar cells and rechargeable batteries. He received a Bachelor's degree in chemistry in 2000 and a Ph.D. degree in physical chemistry in 2005, both from Nankai University. He worked as Endeavour Research Fellow in Queensland University of Technology in 2008, and as a visiting researcher at University of Cambridge from 2014 to 2015.

TOC:

Colloidal Quantum Dot Solar Cells: Progressive Deposition Techniques and Future Prospects on Large-area Fabrication

The possibilities of different deposition techniques which can bring quantum dot (QD)-based solar cells to the industrial level are assessed. With perovskite QDs showing potential to breach the Shockley–Queisser limit based on their unique intrinsic features, the discussions on the challenges for perovskite QD solar cells in particular, are given in an attempt to achieve large-area fabrication for further advancing technology to solve pivotal energy and environmental issues.

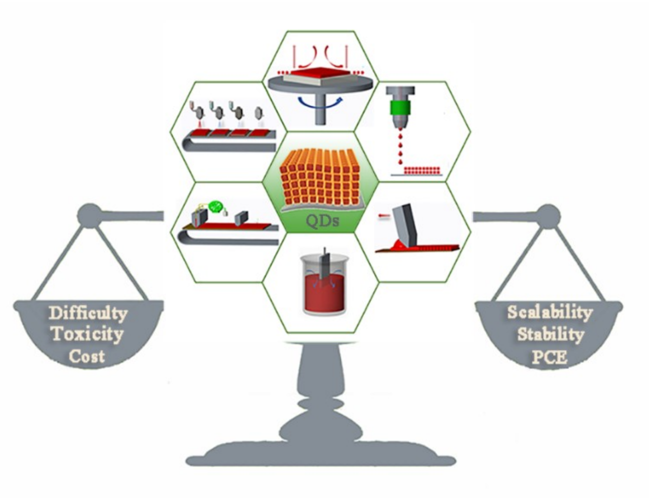
QDs
Difficulty
Toxicity
Cost
Scalability
Stability
PCE